
1 **Multi-model ensemble projection of global dust cycle by the**
2 **end of 21st century using CMIP6 data**

3
4 **Yuan Zhao¹, Xu Yue¹, Yang Cao², Jun Zhu¹, Chenguang Tian¹, Hao Zhou²,**
5 **Yuwen Chen¹, Yihan Hu¹, Weijie Fu¹ and Xu Zhao¹**

6
7 ¹ Jiangsu Key Laboratory of Atmospheric Environment Monitoring and Pollution
8 Control, Collaborative Innovation Center of Atmospheric Environment and Equipment
9 Technology, School of Environmental Science and Engineering, Nanjing University of
10 Information Science & Technology (NUIST), Nanjing, 210044, China

11 ² Climate Change Research Center, Institute of Atmospheric Physics, Chinese Academy
12 of Sciences, Beijing, 100029, China

13
14
15 Corresponding author: Xu Yue (Email: yuexu@nuist.edu.cn)

Formatted: Line spacing: 1.5 lines

Formatted: Line spacing: 1.5 lines

18
19
20
21
22
23
24
25
26
27
28
29
30
31
32
33
34
35
36
37
38
39
40
41
42
43
44
45
46
47

Abstract

As a natural aerosol with the largest emissions on land, dust has important impacts on atmospheric environment and climate systems. Both the emissions and transport of dust aerosols are tightly connected to meteorological conditions and as a result are confronted with strong modulations by the changing climate. Here, we project the changes of global dust emissions and loading by the end of the 21st century using an ensemble of model outputs from the Coupled Model Intercomparison Project version 6 (CMIP6) under four Shared Socioeconomic Pathways (SSPs). Based on the validations against site-level observations, we select 59 out of 1014 models and estimate an ensemble global dust emission of 3314±2566±1996 Tg a⁻¹ (1Tg = 10¹²g) at present day, in which 7568% is dry deposited and 2531% is wet deposited. Compared to 2005-2014, global dust emissions show varied responses with a reduction of 15.8-5.6±503 Tg a⁻¹ under the SSP3-7.0 scenario but increased emissions up to 53.460.7±542 Tg a⁻¹ under the SSP5-8.5 scenario at 2090-2099. For all scenarios, the most significant increase of dust emissions appears in North Africa (0.4%-4.76%-5.6%) due to the combined effects of reduced ~~relative humidity and~~ precipitation but strengthened surface wind. In contrast, all scenarios show decreased emissions in ~~central Asia and Taklimakan and Gobi Deserts~~ (-0.68% to -20%) ~~and Middle East~~ (0 to -2.811.9%) because of the increased precipitation but decreased wind speed regionally. The dust loading shows uniform increases over North Africa (1%-12.6%-13.5%) and the downwind Atlantic following the increased emissions, but decreases over East Asia (-1.3.4% to -15.210.5%) and the downwind Pacific partly due to enhanced local precipitation that promotes wet deposition. ~~As a result~~In total, global dust loading will increase by 2.1%-9.30%-12.5% at the end of the 21st century under different climate scenarios, suggesting a likely strengthened radiative and climatic perturbations by dust aerosols in a warmer climate.

Keywords: CMIP6, dust emissions, concentrations, climate change, ensemble projection

Formatted: Font colour: Text 1
Formatted: Font colour: Text 1

48

49 **1 Introduction**

50 Dust aerosol is one of the major air pollutants with strong climatic and
51 environmental effects. Suspended dust aerosols can absorb and scatter solar radiation,
52 and act as condensation nuclei so as to change the cloud optical properties (~~Tegen et al.,~~
53 ~~2004; Penner et al., 2006; Forster et al., 2008~~)(~~Tegen et al., 2004; Penner et al., 2006;~~
54 ~~Forster et al., 2008~~). Dust deposition can change the albedo of snow and ice and
55 transport mineral elements to the ocean (~~Jickells et al., 2005; Mahowald et al., 2005;~~
56 ~~Wittmann et al., 2017~~)(~~Jickells et al., 2005; Mahowald et al., 2005; Wittmann et al.,~~
57 ~~2017~~). Furthermore, strong dust storms present as a serious threat to human society by
58 reducing road visibility that influences traffic safety (~~Middleton, 2017~~)(~~Middleton,~~
59 ~~2017~~), carrying bacteria and viruses that affects public health (~~Goudie, 2014~~)(~~Goudie,~~
60 ~~2014~~), and reducing crop yields that endangers the food supply (~~Stefanski and~~
61 ~~Sivakumar, 2009~~)(~~Stefanski and Sivakumar, 2009~~). In light of the great impacts of dust
62 on climate and environment, it is of significant importance to study the spatiotemporal
63 characteristics and future changes of global dust aerosols.

64 The dust cycle consists of three major processes including emission, transport, and
65 deposition (~~Schepanski, 2018~~)(~~Schepanski, 2018~~), which are mainly related to
66 meteorological conditions, such as precipitation, humidity, surface wind speed, and
67 turbulent mixing (~~Liu et al., 2004; Shao et al., 2011; Csavina et al., 2014~~)(~~Liu et al.,~~
68 ~~2004; Shao et al., 2011; Csavina et al., 2014~~). Low humidity and/or strong surface wind
69 are in favor of dust emissions (~~Csavina et al., 2014~~)(~~Csavina et al., 2014~~). Atmospheric
70 humidity has a tight coupling effect with soil moisture, which in part controls the
71 threshold of friction velocity and dust emission intensity (~~Munkhtsetseg et al.,~~
72 ~~2016~~)(~~Munkhtsetseg et al., 2016~~). Strong winds and the associated pressure systems
73 promote the momentum of surface layer and consequently increase dust mobilizations
74 (~~Li et al., 2022~~)(~~Li et al., 2022~~). The transport of dust aerosols is related to atmospheric
75 circulation and turbulent mixing, which determine the horizontal and vertical
76 distribution of dust aerosol particles, respectively (~~Zhang et al., 2014; Fernandes et al.,~~
77 ~~2020~~)(~~Zhang et al., 2014; Fernandes et al., 2020~~). The deposition process includes dry

78 and wet settlement, in which the dry deposition is an effective way to remove large
79 particles while wet deposition dominates the removal of fine particles (Breuning-
80 Madsen and Awadzi, 2005; Yue et al., 2009)(Breuning-Madsen and Awadzi, 2005; Yue
81 et al., 2009). Therefore, the spatiotemporal variations of dust aerosols are closely
82 related to meteorological factors.

83 Climate change exerts significant impacts on the global dust cycle. A study using
84 the RegCM3 model showed that dust emissions and the column burden would increase
85 respectively by 2% and 14% in eastern Asia at 2091-2100 relative to 1991-2000 (Zhang
86 et al., 2016)(Zhang et al., 2016). In contrast, the earlier study projected the reductions
87 of dust emissions by 26% using the ECHAM4-OPYC model and 19% using the
88 HADCM3 model in the same region by the midcentury (Tegen et al., 2004)(Tegen et
89 al., 2004). Compared to these studies based on 1-2 models, the ensemble projections
90 using multiple models from the Climate Model Inter-comparison Project (CMIP)
91 showed great potentials of indicating the uncertainties in the estimate of global dust
92 cycle. Wu et al. (2020)Wu et al. (2020) evaluated 15 dust models in CMIP phase 5
93 (CMIP5) and found that the uncertainty was relatively small for the dust belt extending
94 from North Africa to East Asia, but the uncertainties in other regions such as Australia
95 and North America were large. Based on the multi-model ensemble from CMIP5 data,
96 Pu and Ginoux (2018)Pu and Ginoux (2018) estimated an increase of dust optical depth
97 in central Arabian Peninsula and a decrease over northern China in the late half of the
98 21st century under a strong warming scenario. Zong et al. (2021) also projected that dust
99 emissions would decrease in East Asia by the end of 21st century under the same climate
100 scenario. However, the different features of future global dust cycles and the related
101 drivers under varied climate scenarios remain unclear.

102 ~~Compared to CMIP5 models, more dust emission schemes are coupled with~~
103 ~~dynamic vegetation in the CMIP phase 6 (CMIP6)~~The recent phase 6 of CMIP (CMIP6)
104 ~~includes more complete dust variables (e.g., emissions, depositions, concentrations, and~~
105 ~~optical depth) from climate models. The ensemble of CMIP6 simulations has been used~~
106 ~~to depict historical changes in dust cycle and explore the possible climatic drivers (Le~~
107 ~~and Bae, 2022; Li and Wang, 2022). However, this valuable dataset has rarely been~~

108 ~~used for the future projections on the global scale. Compared to CMIP5 models, more~~
109 ~~dust emission schemes are coupled with dynamic vegetation in CMIP6~~ models to
110 optimize land surface emission processes (~~Zhao et al., 2022~~)(~~Zhao et al., 2022~~).
111 ~~However, such~~Such improvement may ~~instead also~~ amplify the uncertainties of dust
112 simulations, because the predicted vegetation change may be inconsistent with the
113 observed tendencies (~~Wu et al., 2020~~)(~~Wu et al., 2020~~). As a result, it is important to
114 validate the simulated present-day dust cycle before the application of different models
115 in the future projection (Aryal and Evans, 2021). In this study, we project the future
116 changes in global dust cycles by the end of 21st century under four different climate
117 scenarios based on the multi-model ensemble mean from CMIP6 models. We select a
118 total of ~~4014~~ climate models providing dust emissions, depositions, and concentrations
119 for all the four scenarios and validate the simulated near-surface dust concentrations ~~at~~
120 ~~18 ground sites and aerosol optical depth (AOD) with site-level measurements.~~ The
121 models with reasonable performance are selected to project future changes in dust
122 emissions and loadings by the years 2090-2099 relative to the present day (2005-2014).
123 The changes in associated meteorological conditions are further explored to identify the
124 main causes of the changes in the global dust cycle.

125

126 **2 Methods and data**

127 2.1 Model data

128 We select all available CMIP6 models (~~last access: April 20th, 2023~~), providing
129 complete variables of dust cycle (emission, dry/wet deposition, and concentration) and
130 the associated meteorology (surface wind, relative humidity, precipitation) for both
131 present day and four future scenarios under the Shared Socioeconomic Pathways (SSPs)
132 of SSP1-2.6, SSP2-4.5, SSP3-7.0, and SSP5-8.5, which represent future climate with
133 the low to high anthropogenic radiative forcings. A total of ~~4014~~ models with different
134 spatial resolutions are selected, ~~including CESM2-WACCM, CNRM-ESM2-1, GFDL-~~
135 ~~ESM4, INM-CM4-8, INM-CM5-0, MIROC6, MIROC-ES2L, MRI-ESM2-0,~~
136 ~~Nor-ESM2-LM, UKESM1-0-LL~~ (Table 1). Different models may have varied numbers
137 of ensemble runs for dust cycle variables (Table S1). ~~To facilitate the comparison, we~~

Formatted

138 ~~select r1i1p1f1 for all models but r1i1p1f2 for models without r1i1p1f1. We use all~~
139 ~~available runs with different variants and labels from each of climate models, resulting~~
140 ~~in a total of 416 runs for every dust variable (120 for history and 296 for four future~~
141 ~~scenarios) and 770 runs for every meteorological variable (212 for history and 558 for~~
142 ~~four future scenarios). In addition, we collect both dust optical depth (DOD) and AOD~~
143 ~~at the historical periods from these models (Table S1). To facilitate the model validation~~
144 ~~and inter-comparison, we interpolate all model data with different spatial resolution to~~
145 ~~the same of $1^\circ \times 1^\circ$. For each model, we average all the ensemble runs under one climatic~~
146 ~~scenario to minimize the uncertainties due to initial conditions. As a result, we derive 5~~
147 ~~ensemble means (1 for history and 4 for future) for each variable of every model,~~
148 ~~leaving the same weight among CMIP6 models.~~ We use the average data from 2005 to
149 2014 to indicate conditions at present day and that from 2090 to 2099 as the future
150 period. We project the changes in dust cycle using the multi-model ensemble median
151 ~~(MEM)~~ values between future and present day, and explore the causes of changes by
152 linking the simulated dust cycle with meteorological variables from individual models.

153

154 2.2 Measurement data

155 We use dust concentrations observed at 18 ground sites operated by University of
156 Miami to validate dust concentrations at the lowest level of the ~~1014~~ models. All these
157 sites are located on the islands with 7 in the Atlantic, 7 in the Pacific, 3 in the Southern
158 Ocean, and 1 in the Indian Ocean. Most of these sites were built near the dust source
159 regions with the longest period of 17 years. Although the observed data are not
160 continuous at all sites, they provide the most valuable spatiotemporal information of
161 global dust concentrations and have been widely used in the evaluations of dust models
162 ~~(Ginoux et al., 2001; Yue et al., 2009; Wu et al., 2020)~~ (Ginoux et al., 2001; Yue et al.,
163 ~~2009; Wu et al., 2020).~~ By comparing with these observations, we select 5 out of 10
164 ~~climate models capturing the reasonable features and magnitude of dust distribution for~~
165 ~~the future projections.~~ We also use the monthly AOD measurements from the Aerosol
166 ~~Robotic Network (AERONET) to validate CMIP6 models. Observed AOD is affected~~
167 ~~by many different components in addition to dust aerosols. We select a total of 19 sites~~

168 with at least one-year records and the simulated DOD-to-AOD ratio larger than 0.6 as
169 indicated by the ensemble of CMIP6 models. In this way, AOD at the selected
170 AERONET sites is more likely dominated by dust aerosols.

172 2.3 Dust emission schemes

173 The vertical emission flux F_i for a specific dust size bin i in most of climate models
174 can be derived using the generic equation:

$$175 F_i = C \cdot \rho_d \cdot E \cdot f_m \cdot \alpha \cdot M_i \quad (1)$$

176 Here, C is a tunable parameter set to derive the reasonable dust climatology in
177 individual models. ρ_d is the density of dust particle. E is the impetus composed of
178 wind friction speed (U_f) above the threshold values (U_{*t}) for saltation. The value of
179 U_{*t} is dependent on soil moisture. f_m is the erodibility potential of bare soil
180 suitable for dust mobilization, which is usually parameterized as the cover fraction of a
181 grid cell excluding snow, ice, lake, and vegetation. α is sandblasting mass efficiency
182 related to clay fraction (%clay). M_i is the mass distribution of the specific dust size
183 bin i . The detailed parameterizations for each component of Equation (1) are shown for
184 5 selected models in Table 2. In general, the main factors influencing dust emissions
185 include wind friction velocity, threshold wind speed, soil moisture, clay content, soil
186 bareness, and dust particle size. These variables are used either as individual factors or
187 in multiple components of Eq. 1. For example, in CESM2-WACCM, CESM2,
188 NorESM2-LM, and UKESM1-0-LL, the clay fraction is used to calculate both
189 sandblasting mass efficiency and the threshold of wind friction speed (Lawrence et al.,
190 2019)(Lawrence et al., 2019). In CNRM-ESM2-1, f_m , soil moisture, and %clay α are
191 combined to calculate U_{*t} rather than acting as individual components of F_i factors
192 in the emission function (Zakey et al., 2006)(Zakey et al., 2006).

194 3 Results

195 3.1 Model validations

196 Fig. 1a shows the spatial distribution of ground-based sites for dust observations.
197 These sites cover a wide range of oceanic areas with different distances to source

198 regions. Compared to observed concentrations, (Fig. 1b), the simulations yield
199 correlation coefficients (R) of ~~0.4130-0.8988~~ for ~~1014~~ climate models, among which
200 ~~712~~ models show R of higher than 0.8. ~~The (Table S2). Meanwhile, the simulations~~
201 ~~show~~ normalized standard deviations (NSD, standard deviation of the model divided
202 by that of the observations) ~~rangeranging~~ from ~~0.407~~ to ~~2.5~~, ~~indicating large differences~~
203 ~~in the simulated magnitude~~ ~~16~~. Compared to observed AOD (Fig. 1d), the simulations
204 yield R of ~~dust concentrations among climate models: 0.26-0.79~~ and NSD of ~~0.28-0.95~~
205 (Table S2). With the validations, we select ~~59~~ models for the ~~further analyses future~~
206 ~~projections~~ including CESM2-WACCM, ~~CESM2~~, CNRM-ESM2-1, GFDL-ESM4,
207 ~~GISS-E2-1-G, GISS-E2-1-H, GISS-E2-2-G,~~ NorESM2-LM and UKESM1-0-LL,
208 ~~which. All of these selected model~~ yield NSD between 0.25 and 1.5 and correlation
209 coefficients higher than ~~0.855~~ against observations ~~of both dust concentrations and~~
210 ~~AOD~~.

211 The ensemble ~~median mean~~ of dust concentrations from ~~59~~ selected CMIP6
212 models is compared to observations at ~~48~~ individual stations (Fig. 2). The models
213 reproduce observed magnitude at 6 sites (Figs 2a-2f) downwind of Saharan dust sources
214 with relative mean biases (RMB) ranging from -40% to ~~2237.4%~~. For these sites, the
215 model ensemble also captures reasonable dust seasonality except for the
216 underestimation of peak values in summer for Barbados (Fig. 2a) and those in spring
217 for Cayenne (Fig. 2b). For the rest sites, the multi-model ensemble prediction
218 overestimates dust concentrations at 1 site in the North Atlantic (Fig. 2g), 3 sites in the
219 southern ocean (Figs 2h-2j), and 3 sites in the central Pacific (Fig. 2k-2m), most of
220 which are far away from dust source regions. In contrast, model simulations
221 underestimate dust concentrations at 1 site in the Indian Ocean (Fig. 2n) and 2 sites at
222 the offshore of East Asia (Figs 2o-2p), ~~likely because climate models underestimate~~
223 ~~source strength in Middle East and Central Asia.~~ In sum, the simulated dust
224 concentrations show smaller spatial gradients than observations.

225 ~~The ensemble mean of AOD from 9 selected CMIP6 models is compared to~~
226 ~~observations at 19 AERONET stations (Fig. 3). For six sites (1-6) in the inner North~~
227 ~~Africa, the model prediction underestimates observed peaks in springtime, especially~~

228 at Bidi Bahn and Djougou. As a result, the ensemble predictions at these sites are lower
229 than observations by at least -20% except for DMN Maine Soroa. For three sites (7-9)
230 along the western coast of North Africa, the model ensemble captures the summertime
231 maximum but tends to slightly overestimate AOD in other seasons. For 9 sites (10-18)
232 in Middle East, the predicted AOD reproduces observed seasonality and magnitude
233 with RMB between -27.7% and 20.7%. However, for the only site (CASLEO) in South
234 America, the model prediction shows much higher AOD than measurements. The
235 validations show that simulated AOD from the selected CMIP6 models agree well with
236 the observed spatial pattern especially at regions near dust sources.

237

Formatted: Indent: First line: 2 ch, Line spacing: 1.5 lines

238 3.2 Dust cycle at present day

239 Based on the selected models, the ensemble median dust emissions, concentrations,
240 and depositions are assessed for 2005-2014 (Fig. 34). About 87% of dust emissions are
241 located in the Northern Hemisphere, with hotspots over North Africa, Middle East, ~~and~~
242 ~~central~~West Asia, and Taklimakan ~~and~~ Gobi Deserts (Fig. 3a4a). The source intensity
243 is much smaller in the Southern Hemisphere, with moderate emissions over Australia,
244 South Africa, and southern South America. The global total dust emission from the
245 ensemble of models is about ~~334~~2566±1996 Tg, to which the emissions from Africa
246 alone contribute by ~~6367~~ % (Table 3). Three (CESM2, CESM2-WACCM, and
247 NorESM2-LM) out of nine models show scattered emissions while the rest show more
248 continuous distribution (Fig. S1).

249 The spatial distribution of dust deposition resemble that of emissions but with
250 much larger coverage. Dry deposition is usually confined to the source regions (Fig.
251 ~~3e4c~~) because dust particles with large size are more likely to settle down and cannot
252 travel far away from the source. In contrast, wet deposition is more dispersed (Fig. ~~3e4d~~)
253 because small particles can be transported long distances to the downwind areas and
254 finally washed out by rain. On the global scale, the annual total dry deposition is
255 ~~2463~~1749±1919 Tg, more than ~~three~~two times of the ~~815~~796±372 Tg by wet deposition.

256 The dust budget (emission minus deposition) shows net sources of ~~376~~386±87 Tg
257 a⁻¹ in Africa and ~~74~~77±32 Tg a⁻¹ in Asia (Table 3 ~~and~~ Table S3). Meanwhile, the ocean

Formatted: Line spacing: 1.5 lines

258 acts as a net sink with the largest strength of -262250 ± 62 Tg a⁻¹ in the Atlantic and the
259 secondary of -138117 ± 47 Tg a⁻¹ in the Indian Ocean due to their vicinity to the source
260 regions on the land. Following the emission pattern, dust loading shows high values
261 (>120 mg m⁻²) around the source regions especially North Africa and decreases
262 gradually towards global oceans (Fig. 3b4b).

263

264 3.3 Projection of future dust emissions

265 We calculate the changes of dust emissions at the end of the 21st century (2090-
266 2099) relative to the present day (2005-2014). Global total emissions increase under
267 three scenarios, with the largest change of $53.460.7 \pm 542$ Tg a⁻¹ ($+1.615.0\%$) in the SSP5-
268 8.5 scenario (Fig. 4d5d). However, the total emissions show a moderate reduction of -
269 $15.85.6 \pm 503$ Tg a⁻¹ (-0.4846%) in the SSP3-7.0 scenario (Fig. 4e5c). The most
270 significant changes are located at the major dust source regions, such as North Africa,
271 Taklimakan and Middle East. Dust emissions in North Africa increase in all four
272 scenarios, though with regional heterogeneous responses and varied magnitude of $4.2-$
273 $498-47.4$ Tg a⁻¹ ($0.6\%-5.6\%$) (Table 4-4.7%). The secondary enhancement is found
274 at Australia with increases of $1.0-9.1-4.3$ Tg a⁻¹ ($2.2\%-20.8\%-10.7\%$) except SSP3-7%
275 ~~under the four scenarios.~~ In contrast, dust emissions in ~~central~~
276 ~~Asia and~~ Taklimakan and Gobi Deserts show decreases of -0.64 to $-18.86.2$ Tg a⁻¹ ($-$
277 0.68% to $-20.011.9\%$), which are stronger than the enhancement in North Africa under
278 the SSP3-7.0 scenario (Table 4). Furthermore, dust emissions over Asia (including
279 Taklimakan, Gobi Deserts, West Asia and Middle East) decrease in most scenarios
280 especially for SSP3-7.0, in which the regional reduction ~~dominates~~ causes the global
281 decline of dust emissions (Fig. 4e-5c). The inter-model variability is much higher than
282 the projected median changes, suggesting the large uncertainties among climate models.

283 We further explore the associated changes in meteorological conditions at the
284 source regions (Fig. 56). For North ~~Ameriea~~ Africa, regional precipitation shows limited
285 changes mild reductions under all four scenarios because even though the baseline
286 rainfall is very low (Fig. S1). The ensemble projections show decreased relative
287 humidity of $-4.50.6\%$ to $-15.43.0\%$ and increased surface wind speed of $0.2\%-01-$

Formatted: Font colour: Text 1

Formatted: Font colour: Text 1

288 0.08 m s^{-1} , 8% over North Africa for all scenarios, contributing to the largest
 289 enhancement of regional dust emissions. Similarly, projections show decreased
 290 precipitation and relative humidity but increased surface wind over South Africa,
 291 resulting in the increase of local emissions. As a comparison, precipitation, relative
 292 humidity, and surface wind all show decreasing trends in Australia, where the dust
 293 emissions increase for almost all scenarios except SSP3-7.0. It indicates that the effect of
 294 drier conditions outweighs the decreased momentum for dust emissions in this specific
 295 region. Among the total of 18 regions (the red labels on Fig. 6) with
 296 increased dust emissions under the four scenarios, 17 labels show decreased relative
 297 humidity by at least 0.5%, 14 labels show decreased precipitation, and 11 labels show
 298 increased wind speed (Fig. 5).

299 In contrast, the future dust emissions decrease in central Asia, Taklimakan and
 300 Gobi Deserts, Middle East and West Asia under most scenarios (Fig. 4). Climate
 301 projections show increased precipitation (Fig. S4-S6) and relative humidity (Fig. S2-S7),
 302 but decreased wind speed (Fig. S3-S8) over the source regions in central Asia and
 303 Taklimakan and Gobi Deserts. All these changes in meteorological conditions tend to
 304 inhibit regional dust mobilization. The most significant reduction of 20.9% occurs
 305 in SSP5-8.5-SSP3-7.0 scenario, in which regional precipitation increases by 0.214 mm
 306 day^{-1} , and surface wind speed decreases by 0.408 m s^{-1} . For Middle East, relative
 307 humidity decreases (Fig. S2) due to limited changes in and West Asia, the slight
 308 increase of precipitation (Fig. S1) under the global warming scenarios. However, such
 309 tendency is outweighed by the moderate increase of surface
 310 wind speed (Fig. S3), leading to a decline of regional dust emissions in Middle East
 311 for most scenarios SSP1-2.6 and SSP2-4.5 (Fig. 6). Specifically, almost all the 10
 312 regions with reduced dust emissions under the four scenarios show
 313 increased regional precipitation but decreased wind speed, though 4 regions (all in
 314 Middle East for the four scenarios) 8 labels show decreased relative humidity (Fig. 5).
 315 It suggests that changes in precipitation and wind speed play more dominant roles
 316 in the changes of dust emissions.

317 We select four main source regions with significant emission changes to where

318 ~~dust emissions are projected to increase by at least 1 Tg a⁻¹ under most of future climatic~~
319 ~~scenarios (Table 4). In these regions, we~~ quantify the sensitivity of dust emissions to
320 ~~perturbations in meteorological perturbations-factors~~ (Fig. 6). ~~In these regions, we~~
321 We find positive correlations between the changes in dust emissions and that of wind
322 speed for all models and scenarios. The largest correlation coefficient of 0.868 is
323 derived over ~~North Africa Taklimakan and Gobi Deserts~~ (Fig. 6a7b). In contrast, ~~both~~
324 ~~precipitation and relative humidity are~~ negatively correlated with dust emissions
325 across models and scenarios, ~~though such correlations are moderate for relative~~
326 ~~humidity in central Asia and Taklimakan~~ (Fig. 6f7). On average, we derive the
327 increases of dust emissions by ~~40.5-114.633.1-123.3~~ Tg per 0.1 m s⁻¹ increase in surface
328 wind (Figs ~~6a-6d~~), ~~8.2-138.7~~ Tg per 1% reduction in relative humidity (Figs ~~6e-6h~~),
329 ~~and 25.6-416.27a-7d~~, and ~~9.6-365.0~~ Tg per 0.1 mm day⁻¹ reduction in precipitation
330 (Figs ~~6i-6l7e-7h~~) over the main dust source regions based on the multi-model ensemble
331 projections. Following these sensitivities, the inter-model spread of meteorological
332 changes leads to the large uncertainties in the projection of future dust emissions.
333 Among the ~~five~~ climate models, UKESM1-0-LL shows the largest reductions of
334 wind speed while the highest enhancement of precipitation in most of source regions,
335 resulting in the largest decline of dust emission for this model under all the four
336 scenarios (Fig. 67). In contrast, CNRM-ESM2-1 exhibits the largest increase of wind
337 speed and the consequent enhancement of dust emissions in North Africa. Meanwhile,
338 CESM2-WACCM yields the highest enhancement of dust emissions in Australia where
339 this model projects ~~the largest protruding~~ reduction of precipitation.

340

341 3.4 Projection of future dust loading

342 The dust column concentrations loading show more continuous changes than dust
343 emissions (Fig. 78). By the end of the 21st century, dust loading increases along the
344 "North Africa-Atlantic-North America" and "Australia-South Africa-South America"
345 belts, but decreases along the "central Asia-East Asia-North Pacific" belt. Such pattern
346 is in general consistent among all four future scenarios with the strongest magnitude
347 under the SSP5-8.5 scenario. The loading in Middle East and West Asia shows mixed

348 responses with increasing trend in the SSP5-8.5 scenario but decreasing trends in other
349 scenarios. ~~On the global scale~~In sum, dust loading increases by ~~0.37-1.65 Tg (2.1%-9-~~
350 ~~668.3 Gg (1.0%-13.5%)~~ with enhancement of column ~~concentrations~~load in most
351 regions except for Asia and its downwind regions (Fig. 78 and Table S2S4).

352 We select four dust source regions and two non-source areas in Asia to analyze
353 the driving factors for the changes in dust loading (Fig. 89). Analyses show positive
354 correlation coefficients ranging from 0.7972 to 0.9290 between dust loading and
355 emissions. In contrast, negative correlations from -0.3312 to -0.7968 are yielded
356 between the loading and precipitation. The higher magnitude of correlations in the
357 former relationship suggests that the changes of emission dominate the variations of
358 dust loading. However, the role of precipitation cannot be ignored as it can magnify the
359 impact of emissions. For example, dust emissions in the source region of South Africa
360 increase by 2.1%-~~17.1~~10.3% under different scenarios (Table 4), while dust loading in
361 this region increases by ~~2.2%-38.3%-53.5%~~ (Table S4S4). The higher enhancement of
362 dust loading than emissions is mainly attributed to the decreased precipitation (Fig.
363 S4S6), which reduces the proportion of wet deposition to the total deposition (Fig.
364 S4S9).

365 For the non-source areas such as East Asia and South Asia, the moderate changes
366 of dust emissions cannot explain the significant reductions in dust loading. Instead, the
367 strong enhancement of regional precipitation (Fig. S4S6) helps promote wet deposition
368 of dust in Asia, leading to the reduced amount of suspended particles (Fig. 78) and the
369 increased percentage of wet-to-total deposition (Fig. S4S9). Studies have projected that
370 global warming tends to enhance East Asian summer monsoon and South Asian
371 summer monsoon, leading to increased precipitation in the middle and low latitudes of
372 Asia (Sabade et al., 2011; Wang et al., 2018; Wu et al., 2022)(Sabade et al., 2011; Wang
373 et al., 2018; Wu et al., 2022). These changes are not favorable for regional dust
374 mobilization but tend to decrease dust loading through increased wet deposition.

375

376 4 Conclusions and discussion

377 Based on the multi-model ensemble approach, our study projected the changes of

378 dust emissions and loadings by the end of 21st century relative to present day. It is found
379 that dust emissions likely increase in Africa and Australia but decrease in Asia. Such a
380 pattern is consistent among different climate scenarios though the magnitude of
381 regional changes show some variations. As a result, the net changes of global dust
382 emissions vary among future scenarios with the moderate changes in SSP3-7.0 due to
383 the strongest emission reduction over Asia, but the large increase of 4.75.0% in SSP5-
384 8.5 because of the prominent dust emission enhancement in Africa. The changes of dust
385 loading in general follow that of emissions but with associated joint impacts of
386 precipitation, which magnify affects the changes of dust loading through less wet
387 deposition. The decreased precipitation may further promote dust loading over regions
388 with increased emissions (e.g. South Africa) but through the reductions in wet
389 deposition. In contrast, increased precipitation decreases dust loading by more wet
390 deposition over regions with increased precipitation moderate or limited changes in
391 dust emissions (e.g., East Asia).

392 Our projection revealed large uncertainties in the future global dust cycle. These
393 uncertainties are firstly originated from the discrepancies in the dust emission schemes
394 and the size bins/ranges employed by different climate models. To limit the negative
395 impacts of model diversity, we validated the simulated low-level dust concentrations
396 and AOD, and selected the models with reasonable performance. The ensemble mean
397 of these selected models could better capture the observed magnitude and distribution
398 of dust concentrations (Fig. and AOD (Figs 2 and 3)). However, such validations
399 excluded half of these several available models, potentially increasing the uncertainties of
400 multi-model ensemble due to the small sample size. Based on the recent evaluations
401 (Wu et al., 2022; Zhao et al., 2022)(Wu et al., 2022; Zhao et al., 2022), the latest version
402 of CMIP models did not improve the performance in the simulated dust cycles,
403 including concentrations, deposition, and optical depth, suggesting that the more
404 validations may rule out even more available models for the future projection. As a
405 result, the observation-based constraint of emission schemes (e.g. adjusting the tunable
406 parameter *C* in Equation 1) and size bins (e.g., extending or reducing the size range) in
407 individual models is a requisite step to reduce the uncertainties in modeling the global

408 dust cycle.

409 ~~Even though the inter-model variability can not be excluded, we applied the multi-~~
410 ~~model ensemble approach to minimize the projection biases from individual models.~~
411 ~~We used the median instead of mean values from the selected models so that our~~
412 ~~projections reflected the tendency of the majority models rather than that of the single~~
413 ~~model with maximum changes. At present day, the ensemble projection reasonably~~
414 ~~captures the observed dust concentrations for most sites. The largest emission from~~
415 ~~Africa accounts for 63% of the global emissions, similar to the estimates by previous~~
416 ~~studies (Wu et al., 2020; Aryal and Evans, 2021; Zhao et al., 2022). The global mean~~
417 ~~burden of 19 Tg is different by 6 Tg to 7 Tg compared to the three datasets used by~~
418 ~~Zhao et al. (2022). In the future, our ensemble projected increases of dust emissions in~~
419 ~~North Africa and Australia while the reductions in central Asia are consistent with the~~
420 ~~results predicted using two different models (Tegen et al., 2004).~~

421 For this study, we did not validate the long-term trend of simulated dust variables
422 due to the data limitations. A recent work by Kok et al. (2023) showed increasing global
423 dust loading during historical periods with the glacier deposition records and found that
424 all the CMIP6 models could not reproduce such tendency. While this newly derived
425 dataset provides a unique aspect for global dust activity, more validations are required
426 using the ground-based concentrations and/or satellite-retrieved AOD. For example, the
427 long-term records in China showed a decreasing trend of dust storm in East Asia during
428 1954-2000 (Wang et al., 2005), inconsistent with the upward trend in the same region
429 as revealed by Kok et al. (2023). Another limitation is that we ignore the possible
430 impacts of vegetation changes on the future dust activity. Previous studies have revealed
431 that dynamic vegetation process could significantly alter future dust activity
432 (Woodward et al., 2022). However, we were not able to identify such effects because
433 CMIP6 models do not output the information of dust sources and their strength. As a
434 check, we compared the changes of dust emissions at vegetation-free grid points for
435 both historical and future periods so as to exclude the impacts of vegetation changes.
436 We found very limited differences for those grids (Table S5) relative to the changes for
437 all grids (Table 4), suggesting that the changes of dust area are limited in most of the
438 CMIP6 models.

439 We applied the multi-model ensemble approach to minimize the projection biases

440 from individual models. We used the median instead of mean values from the selected
441 models so that our projections reflected the tendency of the majority models rather than
442 that of the single model with maximum changes. At present day, the ensemble
443 projection reasonably captures the observed dust concentrations and AOD at most sites
444 (Figs 2-3). The predicted annual dust emissions of 2566±1996 Tg is close to the
445 estimate of 2836 Tg a⁻¹ using an ensemble of five different dust models (Checa-Garcia
446 et al., 2021). The largest emission from Africa accounts for 67% of the global emissions,
447 similar to the estimates by previous studies (Wu et al., 2020; Aryal and Evans, 2021;
448 Zhao et al., 2022). The global burden of 22±8 Tg is close to the range of 12-25 Tg
449 estimated by Zhao et al. (2022) using three different datasets. For the future, our
450 ensemble projected increases of dust emissions in North Africa and Australia while the
451 reductions in central Asia are consistent with the results predicted using two different
452 models (Tegen et al., 2004). The ensemble projections with the 9 selected models (Table
453 4) are in general consistent with the projections using all 14 models (Table S6),
454 especially for the enhancement of dust emissions in the North Africa under all scenarios.
455 However, both projections revealed large inter-model variability that may dampen the
456 significance of the predicted changes.

457 Our sensitivity analyses showed consistent dependence of dust emissions and
458 loadings to meteorological variables among models and scenarios (Figs 67 and 89).
459 With such physical constraints, the trends of dust emissions are determined by the
460 changes of regional to global meteorological fields, especially wind speed and
461 precipitation. For example, models show contrasting tendencies of surface wind over
462 North Africa (Fig. 6a7a) and precipitation in AustraliaMiddle East and West Asia (Fig.
463 647g), leading to large inter-model variability with opposite signs for the changes in
464 dust emissions by the end of 21st century. Given the importance of climatic change, we
465 checked the ensemble changes in precipitation (Fig. S5S10) and surface wind speed
466 (Fig. S6S11) with all available CMIP6 models (32 models as listed in Table S3) and S7).
467 We found that the main features of increased drought and wind speed over North Africa
468 and South Africa while enhanced rainfall over Asia was retained, indicating following
469 the “drier in dry and wetter in wet” pattern due to the land-air interactions through water

Formatted: Line spacing: 1.5 lines

470 [and energy exchange \(Feng and Zhang, 2015\)](#). It indicates that the main patterns of the
471 changes in both dust emissions and loadings in our projections are solid. As a result,
472 we suggest that dust emissions over the main source regions will likely enhance in a
473 warming climate, contributing to the increased dust aerosol particles and radiative
474 perturbations by the end of the 21st century.

475
476 **Data availability.** The model output data from CMIP6 were downloaded from
477 <https://esgf-node.llnl.gov/search/cmip6/>.

478
479 **Author contributions.** XY conceived the study. XY and YZ designed the research,
480 conducted the data analysis and paper writing. YaC, JZ, CT and HZ provided paper
481 writing advices and helped with data analysis procedures. YuC, YH, WF and XZ
482 provided scientific advices. All co-authors contributed to improve the manuscript.

483
484 **Competing interests.** The contact author has declared that none of the authors has any
485 competing interests.

486
487 **Acknowledgements.** This research was ~~jointly~~ supported by the ~~Natural Science~~
488 ~~Foundation of Jiangsu Province (grant no. BK20220031)~~ and the National ~~Natural~~
489 ~~Science Foundation~~ [Key Research and Development Program](#) of China (~~No.~~
490 ~~42275128~~ [grant no. 2019YFA0606802](#)).

491

492 **References**

- 493 Aryal, Y. N. and Evans, S.: Global Dust Variability Explained by Drought Sensitivity
494 in CMIP6 Models, *J. Geophys. Res.: Earth Surf.*, 126, e2021JF006073, doi:
495 10.1029/2021JF006073, 2021.
- 496 [Bauer, S. E. and Koch, D.: Impact of heterogeneous sulfate formation at mineral dust](#)
497 [surfaces on aerosol loads and radiative forcing in the Goddard Institute for Space](#)
498 [Studies general circulation model, *J. Geophys. Res.*, 110, doi:](#)
499 [10.1029/2005jd005870, 2005.](#)
- 500 Breuning-Madsen, H. and Awadzi, T. W.: Harmattan dust deposition and particle size
501 in Ghana, *Catena*, 63, 23-38, doi: 10.1016/j.catena.2005.04.001, 2005.
- 502 [Checa-Garcia, R., Balkanski, Y., Albani, S., Bergman, T., Carslaw, K., Cozic, A.,](#)
503 [Dearden, C., Marticorena, B., Michou, M., van Noije, T., Nabat, P., O'Connor, F.](#)
504 [M., Oliv  , D., Prospero, J. M., Le Sager, P., Schulz, M., and Scott, C.: Evaluation](#)
505 [of natural aerosols in CRESCENDO Earth system models \(ESMs\): mineral dust,](#)
506 [Atmos. Chem. Phys.](#), 21, 10295-10335, doi: 10.5194/acp-21-10295-2021, 2021.
- 507 Csavina, J., Field, J., F  lix, O., Corral-Avitia, A. Y., S  ez, A. E., and Betterton, E. A.:
508 Effect of wind speed and relative humidity on atmospheric dust concentrations in
509 semi-arid climates, *Sci. Total Environ.*, 487, 82-90, doi:
510 10.1016/j.scitotenv.2014.03.138, 2014.
- 511 Dunne, J. P., Horowitz, L. W., Adcroft, A. J., Ginoux, P., Held, I. M., John, J. G.,
512 Krasting, J. P., Malyshev, S., Naik, V., Paulot, F., Shevliakova, E., Stock, C. A.,
513 Zadeh, N., Balaji, V., Blanton, C., Dunne, K. A., Dupuis, C., Durachta, J., Dussin,
514 R., Gauthier, P. P. G., Griffies, S. M., Guo, H., Hallberg, R. W., Harrison, M., He,
515 J., Hurlin, W., McHugh, C., Menzel, R., Milly, P. C. D., Nikonov, S., Paynter, D.
516 J., Ploshay, J., Radhakrishnan, A., Rand, K., Reichl, B. G., Robinson, T.,
517 Schwarzkopf, D. M., Sentman, L. T., Underwood, S., Vahlenkamp, H., Winton,
518 M., Wittenberg, A. T., Wyman, B., Zeng, Y., and Zhao, M.: The GFDL Earth
519 System Model Version 4.1 (GFDL - ESM 4.1): Overall Coupled Model
520 Description and Simulation Characteristics, *J. Adv. Model. Earth Syst.*, 12,
521 e2019MS002015, doi: 10.1029/2019MS002015, 2020.
- 522 Evans, S., Ginoux, P., Malyshev, S., and Shevliakova, E.: Climate - vegetation
523 interaction and amplification of Australian dust variability, *Geophys. Res. Lett.*,
524 43, 11823 - 11830, doi: 10.1002/2016GL071016, 2016.
- 525 [Feng, H. and Zhang, M.: Global land moisture trends: drier in dry and wetter in wet](#)
526 [over land, *Sci Rep*, 5, 18018, doi: 10.1038/srep18018, 2015.](#)
- 527 Fernandes, R., Dupont, S., and Lamaud, E.: Origins of Turbulent Transport
528 Dissimilarity Between Dust and Momentum in Semiarid Regions, *J. Geophys.*
529 *Res.: Atmos.*, 125, e2019JD031247, doi: 10.1029/2019jd031247, 2020.
- 530 Forster, P., Ramaswamy, V., Artaxo, P., Berntsen, T., Betts, R., Fahey, D. W., Haywood,
531 J., Lean, J., Lowe, D. C., Raga, G., Schulz, M., Dorland, R. V., Bodeker, G.,
532 Etheridge, D., Foukal, P., Fraser, P., Geller, M., Joos, F., Keeling, C. D., Keeling,
533 R., Kinne, S., Lassey, K., Oram, D., O'Shaughnessy, K., Ramankutty, N., Reid,
534 G., Rind, D., Rosenlof, K., Sausen, R., Schwarzkopf, D., Solanki, S. K.,
535 Stenchikov, G., Stuber, N., Takemura, T., Textor, C., Wang, R., Weiss, R., Whorf,

536 T., Nakajima, T., Ramanathan, V., Ramaswamy, V., Artaxo, P., Berntsen, T., Betts,
537 R., Fahey, D. W., Haywood, J., Lean, J., Lowe, D. C., Myhre, G., Nganga, J.,
538 Prinn, R., Raga, G., Schulz, M., and Dorland, R. V.: Changes in Atmospheric
539 Constituents and in Radiative Forcing, *Climate Change 2007: The Physical
540 Science Basis*, Cambridge University Press, Cambridge, UK2008.

541 Ginoux, P., Chin, M., Tegen, I., Prospero, J. M., Holben, B., Dubovik, O., and Lin, S.-
542 J.: Sources and distributions of dust aerosols simulated with the GOCART model,
543 *J. Geophys. Res.: Atmos.*, 106, 20255-20273, doi: 10.1029/2000JD000053, 2001.

544 [Ginoux, P., Prospero, J., Torres, O., and Chin, M.: Long-term simulation of global dust
545 distribution with the GOCART model: correlation with North Atlantic Oscillation,
546 *Environmental Modelling & Software*, 19, 113-128, doi: 10.1016/s1364-
547 8152\(03\)00114-2, 2004.](#)

548 Goudie, A. S.: Desert dust and human health disorders, *Environ. Int.*, 63, 101-113, doi:
549 10.1016/j.envint.2013.10.011, 2014.

550 Jickells, T. D., An, Z. S., Andersen, K. K., Baker, A. R., Bergametti, G., Brooks, N.,
551 Cao, J. J., Boyd, P. W., Duce, R. A., Hunter, K. A., Kawahata, H., Kubilay, N.,
552 laRoche, J., Liss, P. S., Mahowald, N., Prospero, J. M., Ridgwell, A. J., Tegen, I.,
553 and Torres, R.: Global Iron Connections Between Desert Dust, Ocean
554 Biogeochemistry, and Climate, *Science*, 308, 67-71, doi:
555 10.1126/science.1105959, 2005.

556 [Kelley, M., Schmidt, G. A., Nazarenko, L. S., Bauer, S. E., Ruedy, R., Russell, G. L.,
557 Ackerman, A. S., Aleinov, I., Bauer, M., Bleck, R., Canuto, V., Cesana, G., Cheng,
558 Y., Clune, T. L., Cook, B. I., Cruz, C. A., Del Genio, A. D., Elsaesser, G. S.,
559 Faluvegi, G., Kiang, N. Y., Kim, D., Lacis, A. A., Leboissetier, A., LeGrande, A.
560 N., Lo, K. K., Marshall, J., Matthews, E. E., McDermid, S., Mezzuman, K., Miller,
561 R. L., Murray, L. T., Oinas, V., Orbe, C., Garcia-Pando, C. P., Perlwitz, J. P., Puma,
562 M. J., Rind, D., Romanou, A., Shindell, D. T., Sun, S., Tausnev, N., Tsigaridis, K.,
563 Tselioudis, G., Weng, E., Wu, J., and Yao, M. S.: GISS-E2.1: Configurations and
564 Climatology, *J Adv Model Earth Syst*, 12, e2019MS002025, doi:
565 10.1029/2019MS002025, 2020.](#)

566 [Kok, J. F., Storelvmo, T., Karydis, V. A., Adebisi, A. A., Mahowald, N. M., Evan, A. T.,
567 He, C., and Leung, D. M.: Mineral dust aerosol impacts on global climate and
568 climate change, *Nature Reviews Earth & Environment*, 4, 71-86, doi:
569 10.1038/s43017-022-00379-5, 2023.](#)

570 Lawrence, D. M., Fisher, R. A., Koven, C. D., Oleson, K. W., Swenson, S. C., Bonan,
571 G., Collier, N., Ghimire, B., Kampenhout, L. v., Kennedy, D., Kluzek, E.,
572 Lawrence, P. J., Li, F., Li, H., Lombardozzi, D., Riley, W. J., Sacks, W. J., Shi, M.,
573 Vertenstein, M., Wieder, W. R., Xu, C., Ali, A. A., Badger, A. M., Bisht, G.,
574 Broeke, M. v. d., Brunke, M. A., Burns, S. P., Buzan, J., Clark, M., Craig, A.,
575 Dahlin, K., Drewniak, B., Fisher, J. B., Flanner, M. G., Fox, A. M., Gentine, P.,
576 Hoffman, F., Keppel-Aleks, G., Knox, R., Kumar, S., Lenaerts, J., Leung, L. R.,
577 Lipscomb, W. H., Lu, Y., Pandey, A., Pelletier, J. D., Perket, J., Randerson, J. T.,
578 Ricciuto, D. M., Sanderson, B. M., Slater, A., Subin, Z. M., Tang, J., Thomas, R.
579 Q., Martin, M. V., and Zeng, X.: The Community Land Model version 5:

580 Description of new features, benchmarking, and impact of forcing uncertainty, J.
581 Adv. Model. Earth Syst., 11, 4245-4287, doi: 10.1029/2018MS001583, 2019.

582 [Le, T. and Bae, D.-H.: Causal influences of El Niño–Southern Oscillation on global](#)
583 [dust activities, Atmos. Chem. Phys., 22, 5253-5263, doi: 10.5194/acp-22-5253-](#)
584 [2022, 2022.](#)

585 Li, J., Hao, X., Liao, H., Yue, X., Li, H., Long, X., and Li, N.: Predominant Type of
586 Dust Storms That Influences Air Quality Over Northern China and Future
587 Projections, Earth's Future, 10, e2022EF002649, doi: 10.1029/2022ef002649,
588 2022.

589 [Li, W. and Wang, Y.: Reduced surface fine dust under droughts over the southeastern](#)
590 [United States during summertime: observations and CMIP6 model simulations,](#)
591 [Atmos. Chem. Phys., 22, 7843-7859, doi: 10.5194/acp-22-7843-2022, 2022.](#)

592 Liu, X., Yin, Z., Zhang, X., and Yang, X.: Analyses of the spring dust storm frequency
593 of northern China in relation to antecedent and concurrent wind, precipitation,
594 vegetation, and soil moisture conditions, J. Geophys. Res., 109, D16210, doi:
595 10.1029/2004JD004615, 2004.

596 Mahowald, N. M., Baker, A. R., Bergametti, G., Brooks, N., Duce, R. A., Jickells, T.
597 D., Kubilay, N., Prospero, J. M., and Tegen, I.: Atmospheric global dust cycle and
598 iron inputs to the ocean, Global Biogeochem. Cycles, 19, GB4025, doi:
599 10.1029/2004GB002402, 2005.

600 Marticorena, B., Bergametti, G., Aumont, B., Callot, Y., N'Doum, C., and Legrand, M.:
601 Modeling the atmospheric dust cycle 2. Simulation of Saharan dust sources, J.
602 Geophys. Res., 102, 4387-4404, doi: 10.1029/96JD02964, 1997.

603 Middleton, N. J.: Desert dust hazards: A global review, Aeolian Res., 24, 53-63, doi:
604 10.1016/j.aeolia.2016.12.001, 2017.

605 Munkhtsetseg, E., Shinoda, M., Gillies, J. A., Kimura, R., King, J., and Nikolich, G.:
606 Relationships between soil moisture and dust emissions in a bare sandy soil of
607 Mongolia, Particuology, 28, 131-137, doi: 10.1016/j.partic.2016.03.001, 2016.

608 Nabat, P., Somot, S., Mallet, M., Michou, M., Sevault, F., Driouech, F., Meloni, D.,
609 Sarra, A. d., Biagio, C. D., Formenti, P., Sicard, M., Léon, J. F., and Bouin, M. N.:
610 Dust aerosol radiative effects during summer 2012 simulated with a coupled
611 regional aerosol–atmosphere–ocean model over the Mediterranean, Atmos. Chem.
612 Phys., 15, 3303–3326, doi: 10.5194/acp-15-3303-2015, 2015.

613 Oleson, K. W., Lawrence, D. M., Flanner, M. G., Kluzek, E., Levis, S., Swenson, S. C.,
614 Thornton, E., Dai, A., Decker, M., Dickinson, R., Feddema, J., Heald, C. L.,
615 Lamarque, J. F., Niu, G., Qian, T., Running, S., Sakaguchi, K., Slater, A., Stöckli,
616 R., Wang, A., Yang, L., Zeng, X., and Zeng, X.: Technical Description of version
617 4.0 of the Community Land Model (CLM)(No. NCAR/TN-478+STR),
618 University Corporation for Atmospheric Research, 266, 10.5065/D6FB50WZ,
619 2010.

620 Penner, J. E., Quaas, J., Storelvmo, T., Takemura, T., Boucher, O., Guo, H., Kirkeva,
621 A., and Seland, Ø.: Model intercomparison of indirect aerosol effects, Atmos.
622 Chem. Phys., 6, 3391–3405, doi: 10.5194/acp-6-3391-2006, 2006.

623 Pu, B. and Ginoux, P.: How reliable are CMIP5 models in simulating dust optical depth?,

624 Atmos. Chem. Phys., 18, 12491-12510, doi: 10.5194/acp-18-12491-2018, 2018.

625 Sabade, S. S., Kulkarni, A., and Kripalani, R. H.: Projected changes in South Asian
626 summer monsoon by multi-model global warming experiments, Theor. Appl.
627 Climatol., 103, 543-565, doi: 10.1007/s00704-010-0296-5, 2011.

628 Schepanski, K.: Transport of Mineral Dust and Its Impact on Climate, Geosciences, 8,
629 151, doi: 10.3390/geosciences8050151, 2018.

630 Shao, Y., Wyrwoll, K. H., Chappell, A., Huang, J., Lin, Z., McTainsh, G. H., Mikami,
631 M., Tanaka, T. Y., Wang, X., and Yoon, S.: Dust cycle: An emerging core theme
632 in Earth system science, Aeolian Res., 2, 181-204, doi:
633 10.1016/j.aeolia.2011.02.001, 2011.

634 Stefanski, R. and Sivakumar, M. V. K.: Impacts of sand and dust storms on agriculture
635 and potential agricultural applications of a SDSWS, IOP Conf. Ser.: Earth
636 Environ. Sci, 7, 012016, doi: 10.1088/1755-1307/7/1/012016, 2009.

637 Tegen, I., Werner, M., Harrison, S. P., and Kohfeld, K. E.: Relative importance of
638 climate and land use in determining present and future global soil dust emission,
639 Geophys. Res. Lett., 31, L05105, doi: 10.1029/2003GL019216, 2004.

640 Wang, S., Wang, J., Zhou, Z., and Shang, K.: Regional characteristics of three kinds of
641 dust storm events in China, Atmos. Environ., 39, 509-520, doi:
642 10.1016/j.atmosenv.2004.09.033, 2005.

643 Wang, T., Miao, J., Sun, J., and Fu, Y.: Intensified East Asian summer monsoon and
644 associated precipitation mode shift under the 1.5 °C global warming target, Adv.
645 Clim. Change Res., 9, 102-111, doi: 10.1016/j.accre.2017.12.002, 2018.

646 Wittmann, M., Groot Zwaafink, C. D., Steffensen Schmidt, L., Guðmundsson, S.,
647 Pálsson, F., Arnalds, O., Björnsson, H., Thorsteinsson, T., and Stohl, A.: Impact
648 of dust deposition on the albedo of Vatnajökull ice cap, Iceland, The Cryosphere,
649 11, 741-754, doi: 10.5194/tc-11-741-2017, 2017.

650 Woodward, S.: Mineral Dust in HadGEM2, Hadley Centre Technical Note, 087, Met
651 Office Hadley Centre, Fitzroy Road, Exeter, EX1 3PB, United Kingdom.
652 <https://library.metoffice.gov.uk/Portal/Default/en-GB/RecordView/Index/2522462011>.

653 Woodward, S., Sellar, A. A., Tang, Y., Stringer, M., Yool, A., Robertson, E., and
654 Wiltshire, A.: The simulation of mineral dust in the United Kingdom Earth
655 System Model UKESM1, Atmos. Chem. Phys., 22, 14503-14528, doi:
656 10.5194/acp-22-14503-2022, 2022.

657 Wu, C., Lin, Z., He, J., Zhang, M., Liu, X., Zhang, R., and Brown, H.: A process-
658 oriented evaluation of dust emission parameterizations in CESM: Simulation of
659 a typical severe dust storm in East Asia, J. Adv. Model. Earth Syst., 8, 1432-1452,
660 doi: 10.1002/2016MS000723, 2016.

661 Wu, C., Lin, Z., and Liu, X.: The global dust cycle and uncertainty in CMIP5 (Coupled
662 Model Intercomparison Project phase 5) models, Atmos. Chem. Phys., 20, 10401-
663 10425, doi: 10.5194/acp-20-10401-2020, 2020.

664 Wu, Q., Li, Q., Ding, Y., Shen, X., Zhao, M., and Zhu, Y.: Asian summer monsoon
665 responses to the change of land-sea thermodynamic contrast in a warming climate:
666 CMIP6 projections, Adv. Clim. Change Res., 13, 205-217, doi:
667 10.1016/j.accre.2022.01.001, 2022.

Formatted: Indent: Left: 0 cm, Hanging: 0.99 cm

668 Yue, X., Wang, H., Wang, Z., and Fan, K.: Simulation of dust aerosol radiative feedback
669 using the Global Transport Model of Dust: 1. Dust cycle and validation, *J.*
670 *Geophys. Res.*, 114, D10202, doi: 10.1029/2008JD010995, 2009.

671 Zakey, A. S., Solmon, F., and Giorgi, F.: Implementation and testing of a desert dust
672 module in a regional climate model, *Atmos. Chem. Phys.*, 6, 4687–4704, doi:
673 10.5194/acp-6-4687-2006, 2006.

674 Zhang, D., Gao, X., Zakey, A., and Giorgi, F.: Effects of climate changes on dust aerosol
675 over East Asia from RegCM3, *Adv. Clim. Change Res.*, 7, 145-153, doi:
676 10.1016/j.accre.2016.07.001, 2016.

677 Zhang, J., Shao, Y., and Huang, N.: Measurements of dust deposition velocity in a wind-
678 tunnel experiment, *Atmos. Chem. Phys.*, 14, 8869-8882, doi: 10.5194/acp-14-
679 8869-2014, 2014.

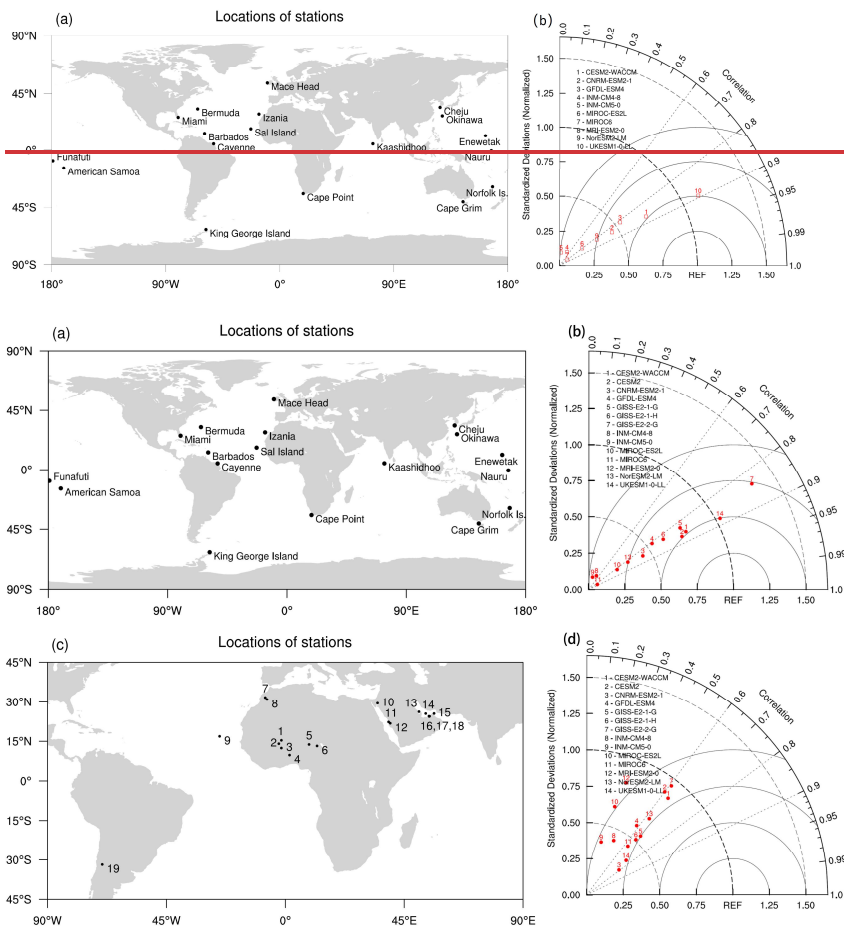
680 Zhao, A., Ryder, C. L., and Wilcox, L. J.: How well do the CMIP6 models simulate dust
681 aerosols?, *Atmos. Chem. Phys.*, 22, 2095-2119, doi: 10.5194/acp-22-2095-2022,
682 2022.

683 Zong, Q., Mao, R., Gong, D., Wu, C., Pu, B., Feng, X., and Sun, Y.: Changes in Dust
684 Activity in Spring over East Asia under a Global Warming Scenario, *Asia-Pac. J.*
685 *Atmos. Sci.*, 57, 839-850, doi: 10.1007/s13143-021-00224-7, 2021.

686

687

Formatted: Line spacing: 1.5 lines

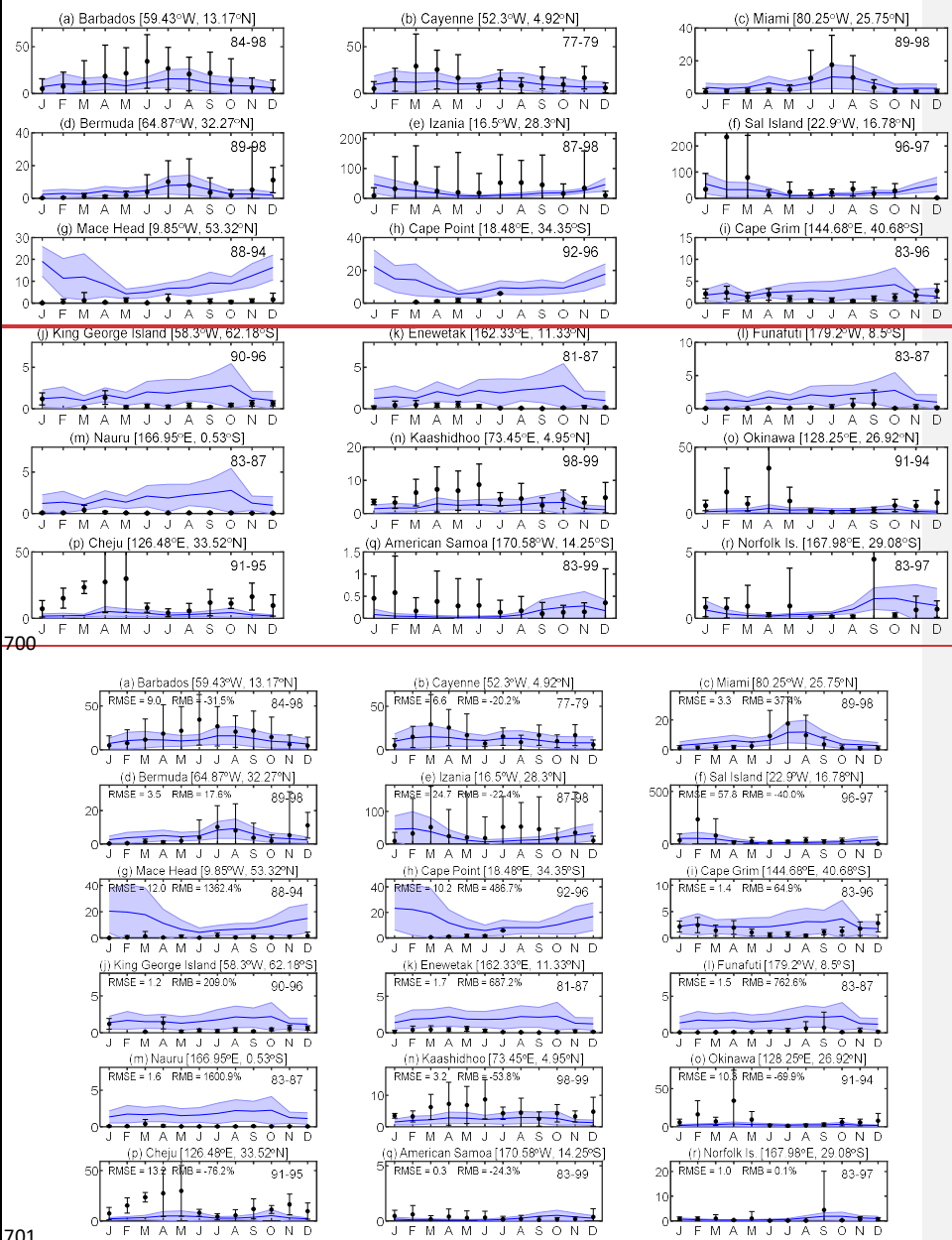


688

689

690 **Figure 1.** (a) Locations of 18 observational stations in the University of
 691 Miami Ocean Aerosol Network and the (b) evaluation of simulated dust concentrations
 692 from CMIP6 models at these stations. (c) Locations of 19 AERONET sites and the (d)
 693 evaluation of simulated AOD from CMIP6 models at these stations. The names of
 694 AERONET sites in (c) are 1-Agoufou, 2-Bidi_Bahn, 3-Ouagadougou, 4-Djougou, 5-
 695 Zinder_Airport, 6-DMN_Maine_Soroa, 7-Ras_El_Ain, 8-Ouarzazate, 9-Calhau, 10-
 696 Eilat, 11-KAUST_Campus, 12-Hada_El-Sham, 13-Bahrain, 14-Abu_Al_Bukhoosh,
 697 15-Dhadnah, 16-Mussafa, 17-Dhabi, 18-Masdar Institute, 19-CASLEO. The
 698 longitudes and latitudes of these sites are indicated on Figures 2 and 3.

699



702 **Figure 2.** Comparison of monthly dust concentrations (units: $\mu\text{g m}^{-3}$) between ensemble
 703 simulations by CMIP6 models and observations at 18 sites. The solid lines represent
 704 ensemble mean of simulations with shadows indicating inter-model spread. The points

705 are the monthly mean of observations with errorbars indicating year-to-year variability.

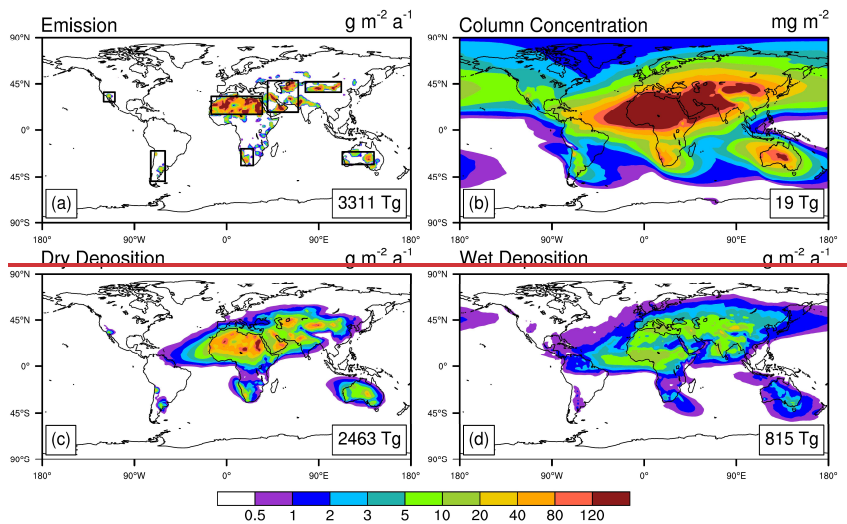
706 The time span of observations at each site is shown in the upper right corner of each

707 panel. Root mean square error (RMSE) and relative mean biases (RMB) of observations

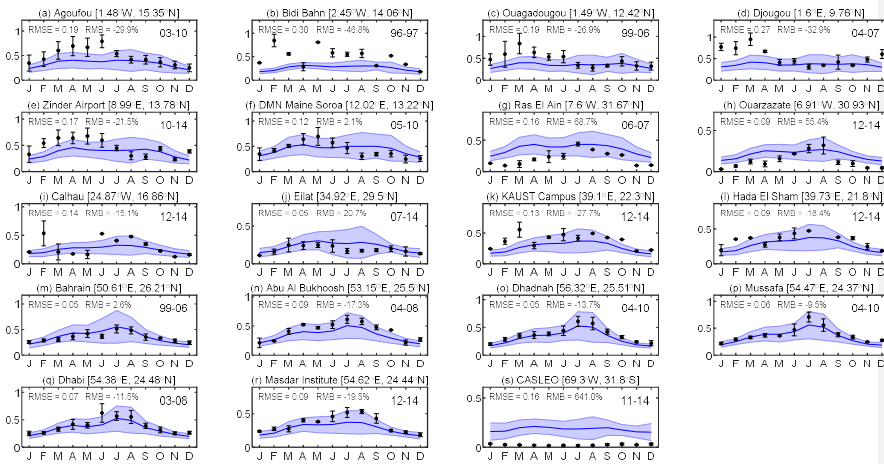
708 and simulations are shown in the upper left corner of each panel.

709

Formatted: Font: Times New Roman



710
711
712

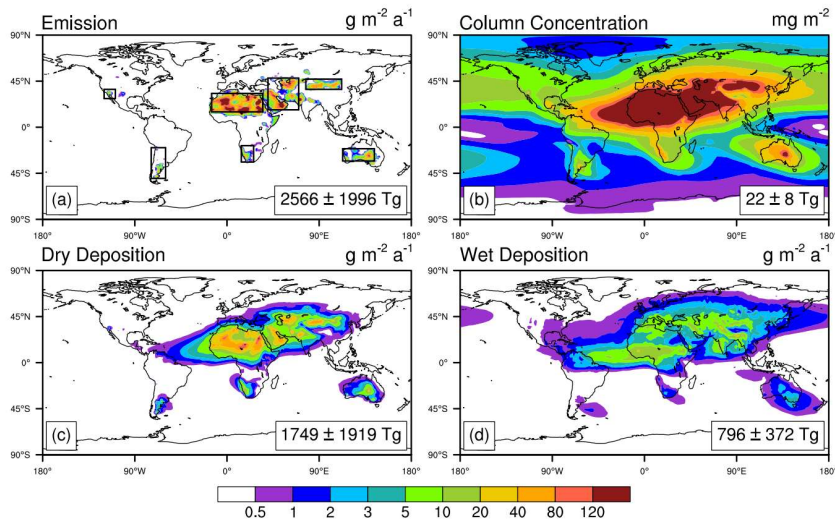


713

714 **Figure 3.** The same as Figure 2 but for the validation of the ensemble simulated aerosol
715 optical depth at 19 AERONET sites.

716
717

Formatted: Font: Bold



718

719 **Figure 4.** Multi-model ensemble of (a) emissions, (b) column concentration, (c)
 720 dry deposition, and (d) wet deposition of dust aerosols at present day (2005-2014). The
 721 box regions on (a) are dust sources of North Africa (NAF) (15°N-33°N, 15°W-35°E),
 722 Middle East (MEA), central and West Asia and (MEWA) (17°N-48°N, 40°E-70°E),
 723 Taklimakan (CA and Gobi Deserts (TGD)) (37°N-47°N, 77°E-112°E), Australia (AUS)
 724 (33°S-21°S, 113°E-144°E), North America (NAM) (28°N-37°N, 120°W-109°W),
 725 South America (SAM) (50°N-20°N, 74°S-60°S), and South Africa (SAF) (34°S-18°S,
 726 14°E-26°E). The detailed results for individual models are shown in Fig. S7S1.

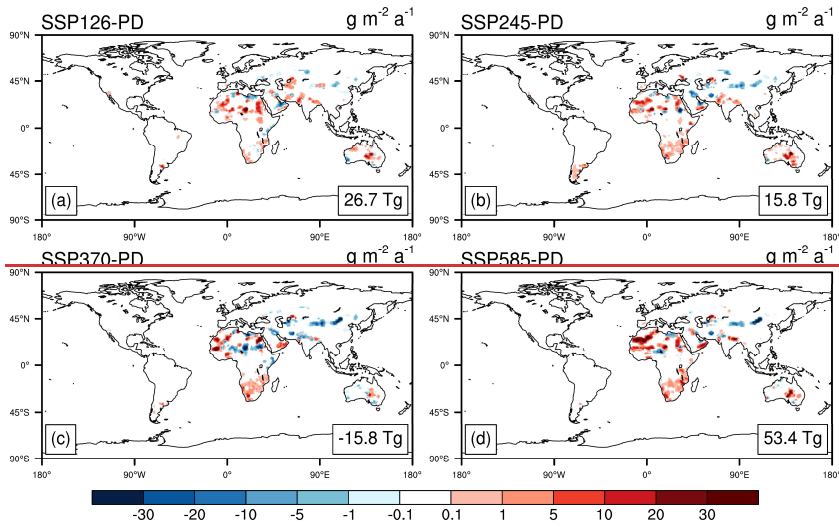
727

728

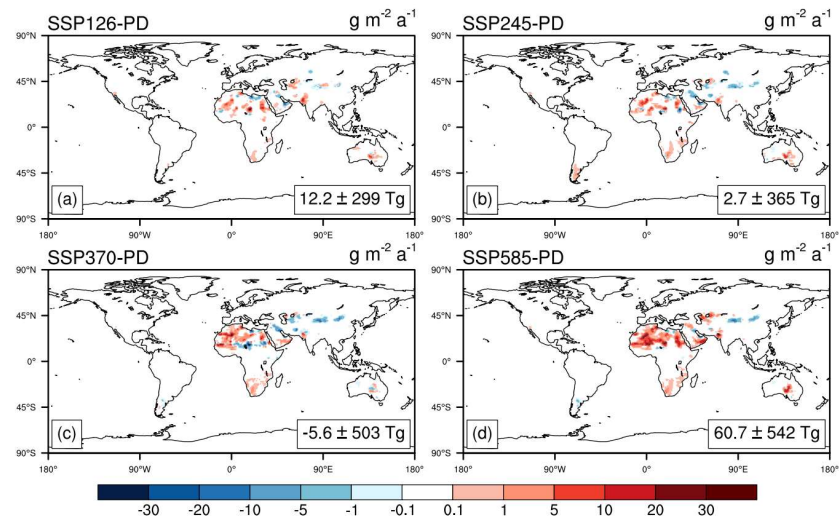
729

730

Formatted: Line spacing: 1.5 lines



731



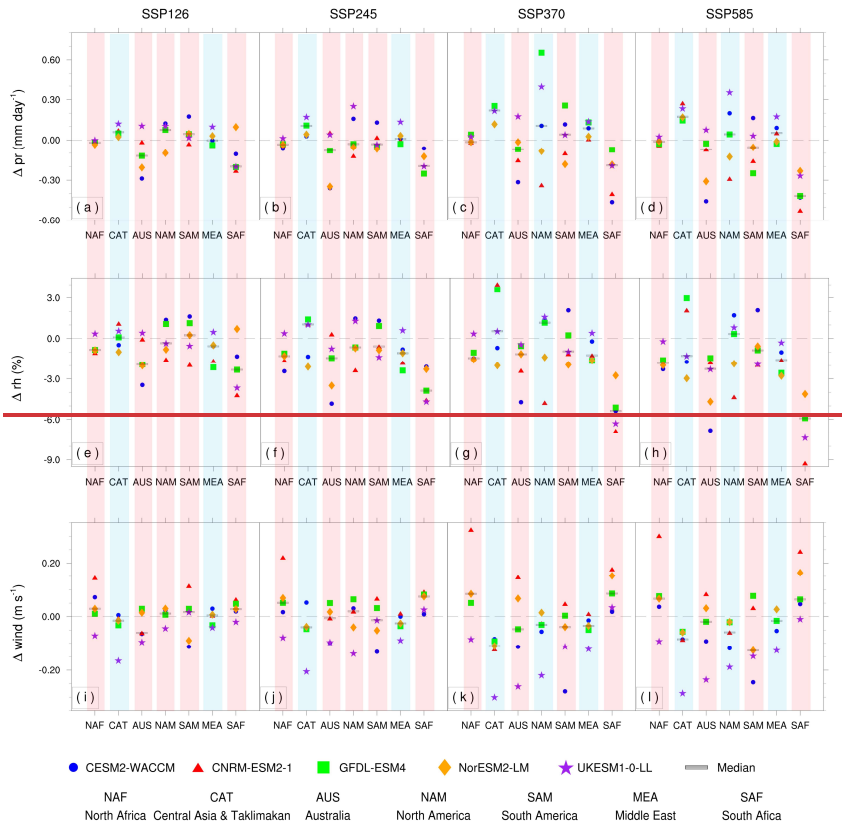
732

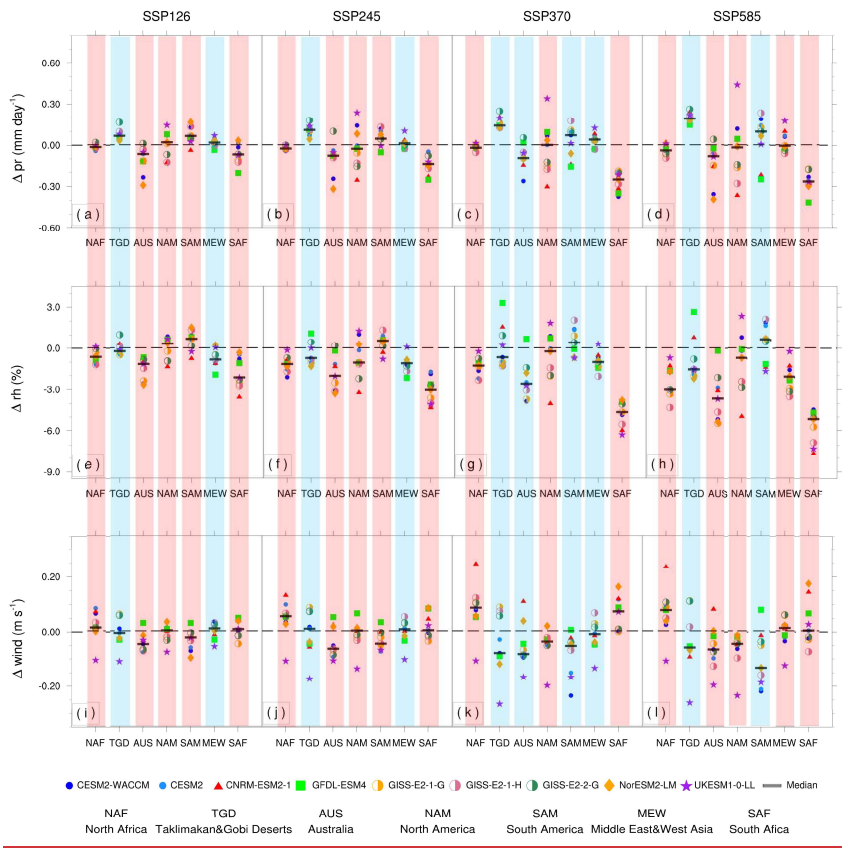
733 **Figure 45.** Multi-model ensemble projection of the changes in dust emissions by the
 734 end of 21st century (2090-2099) relative to present day (2005-2014) under four different
 735 anthropogenic emission scenarios. The detailed projections at 2090-2099 for individual
 736 models are shown in Fig. S8-S11S2-S5 under four different scenarios.

737

738

739





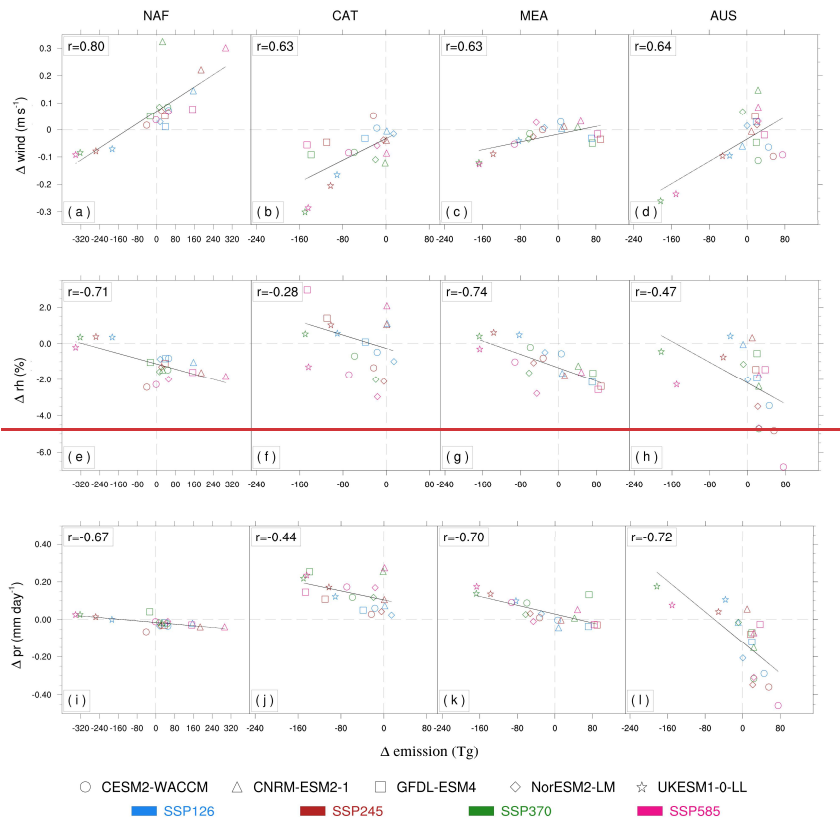
742

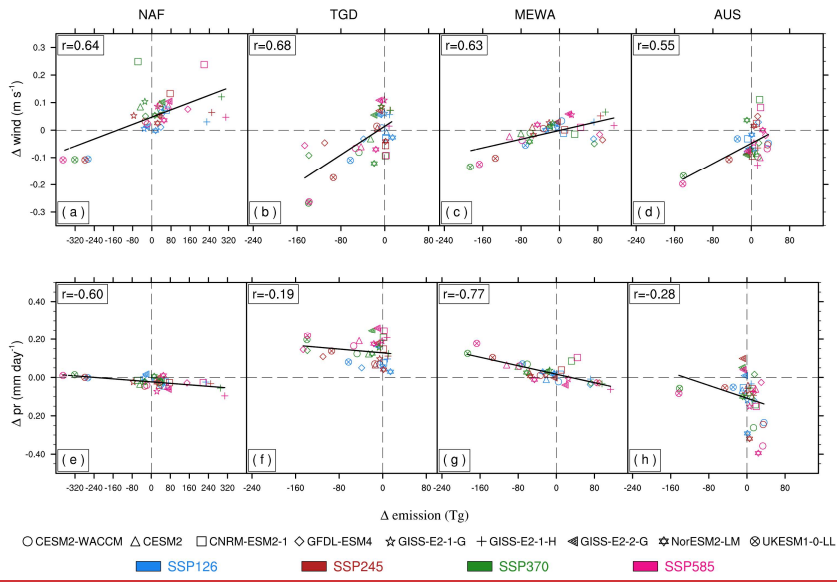
743 **Figure 56.** Changes of meteorological factors over main dust emission regions under
 744 four SSP scenarios by the end of 21st century (2090-2099) relative to present day (2005-
 745 2014). Each box column represents a future climate scenario, including SSP1-2.6,
 746 SSP2-4.5, SSP3-7.0 and SSP5-8.5. Each row represents a meteorological factor,
 747 including precipitation (top), relative humidity (middle), and surface wind (bottom).
 748 Regions with emissions increasing are marked with light red bars, while regions with
 749 emissions decreasing are marked with light blue bars.

750

751

Formatted: Line spacing: 1.5 lines



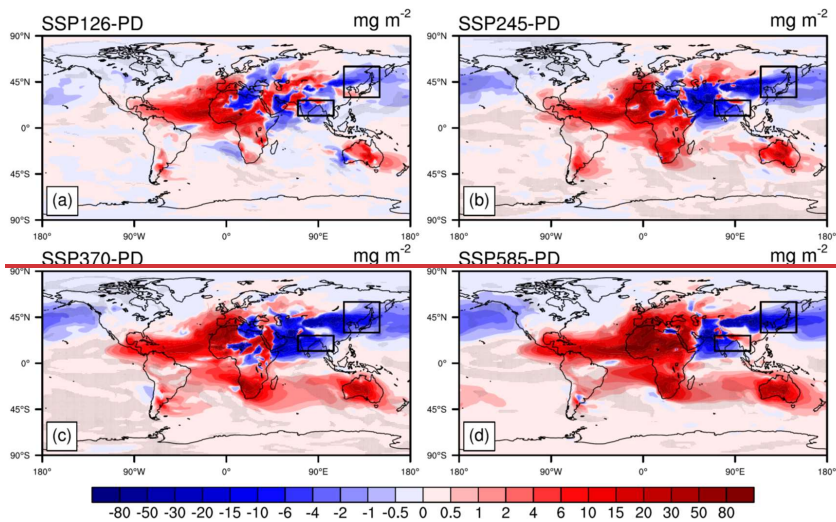


753

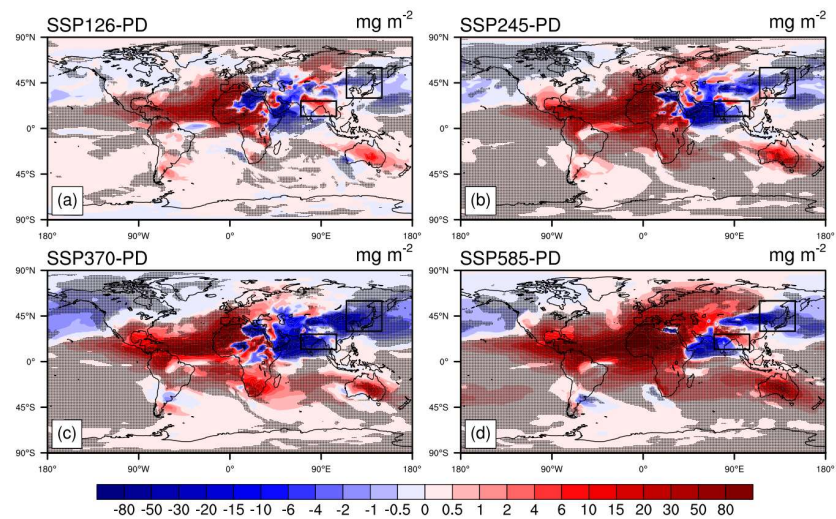
754 **Figure 67.** Relationships between the changes of dust emissions and the changes of
 755 meteorological factors. Each column represents a source region, including North Africa
 756 (NAF), ~~central Asia and Taklimakan (CA and Gobi Deserts (TGD)~~, Middle East
 757 (~~MEA and West Asia (MEWA)~~), and Australia (AUS). Each row represents a
 758 meteorological factor, including surface wind (top), ~~relative humidity (middle),~~ and
 759 precipitation (bottom).

760

Formatted: Font: +Body (Calibri)



761



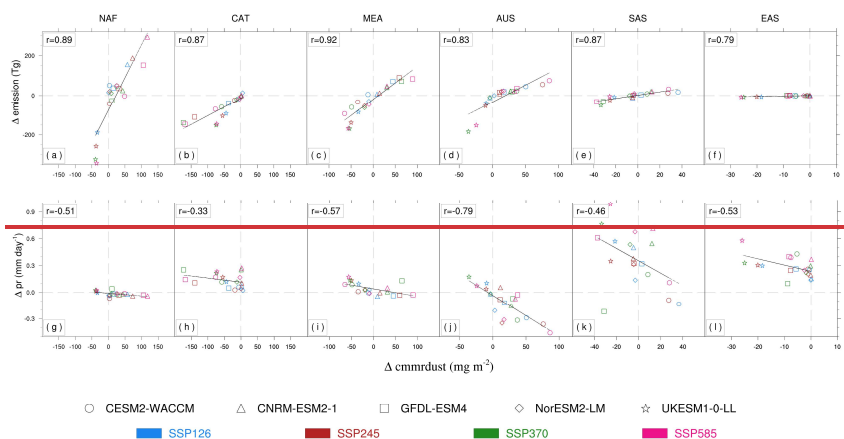
762

763 **Figure 78.** Multi-model ensemble projection of the changes in dust column
 764 concentrationsload by the end of 21st century (2090-2099) relative to present day (2005-
 765 2014). Dotted areas represent changes significant at 90% level. Two additional box
 766 areas are selected for South Asia (12°N - 27°N , 70°E - 105°E) and East Asia- (30°N -
 767 60°N , 115°E - 150°E).

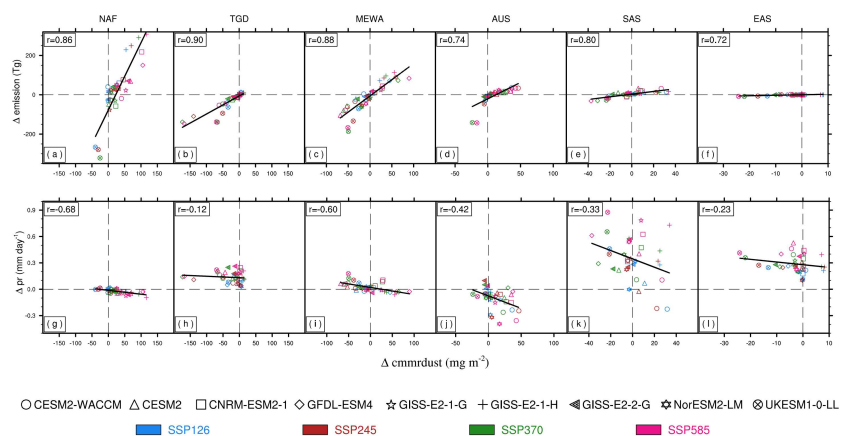
768

769

770



771



772

773 **Figure 89.** Relationships between the changes of dust column concentrations and load
 774 and the change of influencing factors. From left to right, each column represents a specific
 775 region including North Africa (NAF), central Asia and Taklimakan (CAT and Gobi
 776 Deserts (TGD), Middle East (MEA and West Asia (MEWA)), Australia (AUS), South
 777 Asia (SAS) and East Asia (EAS). Each row represents an influencing factor, including
 778 dust emissions (top) and precipitation (bottom).

779

780

781

Formatted: Line spacing: 1.5 lines

782

Table 1. The information of CMIP6 models

Model ^a	Nation	Resolution	Number of runs for dust cycle				
			Hist	SSP126	SSP245	SSP370	SSP585
CESM2-WACCM	U.S.	1.25°×0.94°	<u>3</u>	<u>1</u>	<u>5</u>	<u>3</u>	<u>5</u>
CESM2	U.S.	1.25°×0.94°	11	3	3	3	3
CNRM-ESM2-1	France	1.4°×1.4°	<u>3</u>	<u>5</u>	<u>10</u>	<u>5</u>	<u>5</u>
GFDL-ESM4	U.S.	1.25°×1°	<u>1</u>	<u>1</u>	<u>1</u>	<u>1</u>	<u>1</u>
GISS-E2-1-G	U.S.	2.5°×2°	19	10	25	17	10
GISS-E2-1-H	U.S.	2.5°×2°	10	5	5	1	5
GISS-E2-2-G	U.S.	2.5°×2°	5	5	5	5	5
INM-CM4-8	Russia	2°×1.5°	<u>1</u>	<u>1</u>	<u>1</u>	<u>1</u>	<u>1</u>
INM-CM5-0	Russia	2°×1.5°	<u>10</u>	<u>1</u>	<u>1</u>	<u>5</u>	<u>1</u>
MIROC-ES2L	Japan	2.8°×2.8°	<u>31</u>	<u>10</u>	<u>30</u>	<u>10</u>	<u>10</u>
MIROC6	Japan	1.4°×1.4°	<u>10</u>	<u>3</u>	<u>3</u>	<u>3</u>	<u>3</u>
MRI-ESM2-0	Japan	1°×1°	<u>12</u>	<u>5</u>	<u>10</u>	<u>5</u>	<u>6</u>
NorESM2-LM	Norway	2°×2°	<u>1</u>	<u>1</u>	<u>13</u>	<u>1</u>	<u>1</u>
UKESM1-0-LL	U.K.	1.875°×1.25°	<u>3</u>	<u>5</u>	<u>5</u>	<u>3</u>	<u>4</u>
Total runs			120	56	117	63	60

783

784 ^a The models selected for future projections are bolded.

785

Inserted Cells

Merged Cells

Merged Cells

Merged Cells

Merged Cells

Formatted Table

Inserted Cells

Inserted Cells

Inserted Cells

Inserted Cells

Inserted Cells

Formatted: Line spacing: 1.5 lines

Formatted Table

Inserted Cells

Inserted Cells

Formatted: Line spacing: 1.5 lines

Formatted Table

Inserted Cells

Inserted Cells

Formatted: Line spacing: 1.5 lines

Inserted Cells

Inserted Cells

Formatted: Line spacing: 1.5 lines

Formatted: Line spacing: 1.5 lines

Formatted: Line spacing: 1.5 lines

Formatted: Line spacing: 1.5 lines

Formatted: Line spacing: 1.5 lines

Formatted: Line spacing: 1.5 lines

Formatted: Line spacing: 1.5 lines

Model	E	M_t	f_m	%clay	Reference
CESM2-WACCM	$U_f^2(1 - \frac{U_t}{U_f})(1 + \frac{U_t}{U_f})^2$	3-source-modes, 4 dust-bins	Fraction of grid-cell-excluding snow, lake-and vegetation;- depends on liquid-water and ice contents in top-soil layer	Used to calculate the sandblasting mass efficiency and U_t	Oleson et al. (2010)
NorESM2-LM					Wu et al. (2016)
UKESM1-0-LL	$U_f^3(1 + \frac{U_t}{U_f})(1 - (\frac{U_t}{U_f})^2)$	9 dust-bins	Considering grid-cell-fractions of vegetation		Woodward, (2011)
CNRM-ESM2-1		3 dust-bins	Using roughness-length	Used to calculate the U_t	Marticorena et al. (1997) Zakey et al. (2006) Nabat et al. (2015)
GFDL-ESM4	$U_f^2(U_f - U_t)$	5 dust-bins	Using leaf area index and stem area index	λ	Evans et al. (2016) Dunne et al. (2020)

786

787

Table 2. The parameterization schemes of dust emission function

788

789

790

Formatted: Font: +Body (Calibri), 10.5 pt

Formatted: Line spacing: 1.5 lines

791
792

Table 3. The summary of dust cycle at present day

RegionModel	Emission	Dry-Deposition	Wet-Deposition	Budget*	References
	$Tg\ a^{-1}E_a$	$Tg\ a^{-1}M_d$	$Tg\ a^{-1}f_{mk}$	$Tg\ a^{-1}\%clay_a$	
AfricaCESM2-WACCM	$2171-U_f^3(1-\frac{u_{st}}{u_f})(1+\frac{u_{st}}{u_f})^2$	1541-3 source modes, 4 dust bins	254 Fraction of grid cell excluding snow, lake and vegetation; depends on liquid water and ice contents in top soil layer	376—Used to calculate the sandblasting mass efficiency and U_{st}	Oleson et al. (2010) Wu et al. (2016)
AsiaCESM2	893	591	231	71	
AustraliaNorESM2-LM	255	182	27	45	
South America		80	47	22	11
North-AmericaUKESM1-0-LL	$26-U_f^3(1+\frac{u_{st}}{u_f})(1-(\frac{u_{st}}{u_f})^2)$	20	9 dust bins	-2-Considering grid cell fractions of vegetation	Woodward, 2011
Europe		6	14	32	-40
CNRM-ESM2-1		3 dust bins	Using roughness length	Used to calculate the Pacific Ocean U_{st}	Marticorena et al. (1997) Zakey et al. (2006) Nabat et al. (2015)

Inserted Cells ... [11]
Formatted ... [2]
Formatted ... [1]
Formatted ... [4]
Formatted ... [8]
Formatted ... [10]
Formatted ... [3]
Formatted ... [7]
Formatted ... [9]
Formatted ... [6]
Formatted ... [5]
Merged Cells ... [18]
Merged Cells ... [20]
Formatted ... [21]
Merged Cells ... [16]
Merged Cells ... [14]
Formatted ... [12]
Formatted ... [15]
Formatted ... [13]
Formatted ... [17]
Formatted ... [22]
Formatted ... [19]
Formatted ... [24]
Formatted ... [25]
Formatted ... [26]
Formatted ... [27]
Formatted ... [29]
Formatted ... [23]
Formatted ... [28]
Formatted ... [30]
Formatted ... [32]
Formatted ... [33]
Formatted ... [34]
Formatted ... [36]
Formatted ... [35]
Formatted ... [31]
Deleted Cells ... [43]
Formatted ... [37]
Formatted Table ... [38]
Merged Cells ... [40]
Formatted ... [41]
Formatted ... [44]
Formatted ... [45]
Inserted Cells ... [49]
Inserted Cells ... [48]
Formatted ... [42]
Formatted ... [46]
Formatted ... [39]
Formatted ... [47]
Deleted Cells ... [60]
Deleted Cells ... [61]
Deleted Cells ... [62]
Formatted ... [55]
Inserted Cells ... [53]
Inserted Cells ... [54]
Inserted Cells ... [50]
Formatted ... [56]
Formatted Table ... [51]
Inserted Cells ... [52]

the Indian Ocean	$U_f^2(U_f - U_{st})$	dust bins	Using leaf area index and stem area index	-138	Evans et al. (2016)			
ESM4					Dunne et al. (2020)			
GISS-E2	$U_f^2(U_f - U_{st})$	dust bins	Used to calculate the Atlantic Ocean U_{st}		Ginoux et al. (2004)	115	147	262
					Bauer and Koch (2005)			
					Kelley et al. (2020)			
the Arctic Ocean				0.3		2.1		-2.4

793
794
795

- Formatted: Position: Horizontal: Centre, Relative to: Margin, Vertical: 0.61 cm, Relative to: Paragraph, Horizontal: 0.32 cm, Wrap Around
- Inserted Cells
- Formatted: Font: 9 pt
- Formatted: Widow/Orphan control, Position: Horizontal: Centre, Relative to: Margin, Vertical: 0.61 cm, Relative to: Paragraph, Horizontal: 0.32 cm, Wrap Around
- Formatted: Font: 9 pt, Font colour: Black
- Formatted: Font: 9 pt
- Formatted: Font: 9 pt, Font colour: Black
- Formatted: Font: 9 pt
- Formatted: Font: 9 pt
- Deleted Cells
- Deleted Cells
- Deleted Cells
- Formatted: Widow/Orphan control, Position: Horizontal: Centre, Relative to: Margin, Vertical: 0.61 cm, Relative to: Paragraph, Horizontal: 0.32 cm, Wrap Around
- Inserted Cells
- Formatted: Font: 9 pt
- Inserted Cells
- Inserted Cells
- Inserted Cells
- Formatted Table
- Formatted: Don't adjust right indent when grid is defined, Widow/Orphan control, Don't snap to grid, Position: Horizontal: Centre, Relative to: Margin, Vertical: 0.61 cm, Relative to: Paragraph, Horizontal: 0.32 cm, Wrap Around
- Formatted: Font: 9 pt
- Formatted: Font: 9 pt

796
797

Table 3. The summary of dust cycle at present day*

<u>Region</u>	<u>Emission</u>	<u>Dry Deposition</u>	<u>Wet Deposition</u>	<u>Budget**</u>
	<u>Tg a⁻¹</u>	<u>Tg a⁻¹</u>	<u>Tg a⁻¹</u>	<u>Tg a⁻¹</u>
<u>Africa</u>	<u>1713±1288</u>	<u>1091±1235</u>	<u>236±155</u>	<u>386±87</u>
<u>Asia</u>	<u>736±458</u>	<u>432±419</u>	<u>226±161</u>	<u>77±32</u>
<u>Australia</u>	<u>165±237</u>	<u>110±211</u>	<u>20±25</u>	<u>35±13</u>
<u>South America</u>	<u>52±106</u>	<u>30±63</u>	<u>21±23</u>	<u>1±30</u>
<u>North America</u>	<u>15±27</u>	<u>13±31</u>	<u>9±20</u>	<u>-6±25</u>
<u>Europe</u>	<u>5±3</u>	<u>12±4</u>	<u>34±15</u>	<u>-41±19</u>
<u>Pacific Ocean</u>	<u>/</u>	<u>14±12</u>	<u>48±23</u>	<u>-62±33</u>
<u>Indian Ocean</u>	<u>/</u>	<u>46±23</u>	<u>71±36</u>	<u>-117±47</u>
<u>Atlantic Ocean</u>	<u>/</u>	<u>95±39</u>	<u>155±57</u>	<u>-250±62</u>
<u>Arctic Ocean</u>	<u>/</u>	<u>0±0.3</u>	<u>2±1</u>	<u>-3±1</u>

798 * Values from individual climate models are shown in Table S3

799 **Budget = Emission - Dry Deposition - Wet Deposition

800
801
802
803
804

Formatted: Indent: First line: 0 ch

Formatted: Line spacing: 1.5 lines

805 **Table 4.** Multi-model ensemble projection of the absolute (Tg a⁻¹) and relative
 806 changes (%) in dust emissions by the end of this century (2090-2099)

Region	SSP1-2.6		SSP2-4.5		SSP3-7.0		SSP5-8.5	
	Absolute	Relative	Absolute	Relative	Absolute	Relative	Absolute	Relative
NAF	1910.1 ±121.7	1.82	1053 ±131.4	1.06	4.28±148.0	0.46	4947.4±178.8	4.75
CATIGD					17.7		18.8	
MEAMEWA	-0.64±23.5	-0.68	-2.51±41.3	-5.49	6.2±53.6	18.811.9	4.6±55.7	-20.08.9
AUS	-0.67±43.1	-0.23	4.5±66.4	-2.51.8	4.4±81.1	-21.8	-0.16.8±87.2	0.02.7
NAM	3.8-1.1±17.0	2.8.7	92.1±20.7	20.75.1	-0.1.0±47.2	2.2-0.4	8.74.3±51.6	19.10.7
SAM	0.103±4.7	3.12.2	0.002±6.1	0.41.3	0.001±5.4	-1.40.8	0.002±5.7	-1.3.9
SAF	1.10.02±32.3	14.90.3	0.74±42.1	10.46.7	-0.1±31.3	4.6-2.0	-0.04±27.7	0.6

807 * The **seepedomain** of each region is shown in Figure 1a

808
809
810

- Formatted ... [63]
- Formatted ... [65]
- Formatted ... [67]
- Formatted ... [64]
- Formatted ... [66]
- Formatted ... [68]
- Formatted ... [69]
- Formatted ... [70]
- Formatted ... [71]
- Formatted ... [72]
- Formatted ... [78]
- Formatted ... [79]
- Formatted ... [80]
- Formatted ... [73]
- Formatted ... [74]
- Formatted ... [75]
- Formatted ... [76]
- Formatted ... [77]
- Formatted ... [81]
- Formatted ... [85]
- Formatted ... [87]
- Formatted ... [82]
- Formatted ... [83]
- Formatted ... [84]
- Formatted ... [86]
- Formatted ... [88]
- Formatted ... [89]
- Formatted ... [91]
- Formatted ... [92]
- Formatted ... [90]
- Formatted ... [93]
- Formatted ... [94]
- Formatted ... [95]
- Formatted ... [96]
- Formatted ... [98]
- Formatted ... [99]
- Formatted ... [100]
- Formatted ... [101]
- Formatted ... [102]
- Formatted ... [103]
- Formatted ... [104]
- Formatted ... [105]
- Formatted ... [97]
- Formatted ... [107]
- Formatted ... [108]
- Formatted ... [109]
- Formatted ... [110]
- Formatted ... [111]
- Formatted ... [112]
- Formatted ... [113]
- Formatted ... [106]
- Formatted ... [115]
- Formatted ... [116]
- Formatted ... [117]
- Formatted ... [118]
- Formatted ... [119]
- Formatted ... [120]
- Formatted ... [121]
- Formatted ... [122]

Page 37: [1] Formatted Yuan Zhao 16/05/2023 10:41:00

Widow/Orphan control, Position: Horizontal: Centre, Relative to: Margin, Vertical: 0.61 cm, Relative to: Paragraph, Horizontal: 0.32 cm, Wrap Around

Page 37: [2] Formatted Yuan Zhao 16/05/2023 10:41:00

Font: 9 pt

Page 37: [3] Formatted Yuan Zhao 16/05/2023 10:41:00

Widow/Orphan control, Position: Horizontal: Centre, Relative to: Margin, Vertical: 0.61 cm, Relative to: Paragraph, Horizontal: 0.32 cm, Wrap Around

Page 37: [4] Formatted Yuan Zhao 16/05/2023 10:41:00

Font: 9 pt

Page 37: [5] Formatted Yuan Zhao 16/05/2023 10:41:00

Widow/Orphan control, Position: Horizontal: Centre, Relative to: Margin, Vertical: 0.61 cm, Relative to: Paragraph, Horizontal: 0.32 cm, Wrap Around

Page 37: [6] Formatted Yuan Zhao 16/05/2023 10:41:00

Font: 9 pt

Page 37: [7] Formatted Yuan Zhao 16/05/2023 10:41:00

Widow/Orphan control, Position: Horizontal: Centre, Relative to: Margin, Vertical: 0.61 cm, Relative to: Paragraph, Horizontal: 0.32 cm, Wrap Around

Page 37: [8] Formatted Yuan Zhao 16/05/2023 10:41:00

Font: 9 pt

Page 37: [9] Formatted Yuan Zhao 16/05/2023 10:41:00

Widow/Orphan control, Position: Horizontal: Centre, Relative to: Margin, Vertical: 0.61 cm, Relative to: Paragraph, Horizontal: 0.32 cm, Wrap Around

Page 37: [10] Formatted Yuan Zhao 16/05/2023 10:41:00

Font: 9 pt

Page 37: [11] Inserted Cells Yuan Zhao 16/05/2023 10:41:00

Inserted Cells

Page 37: [12] Formatted Yuan Zhao 16/05/2023 10:41:00

Widow/Orphan control, Position: Horizontal: Centre, Relative to: Margin, Vertical: 0.61 cm, Relative to: Paragraph, Horizontal: 0.32 cm, Wrap Around

Page 37: [13] Formatted Yuan Zhao 16/05/2023 10:41:00

Font: 9 pt, Font colour: Black

Page 37: [14] Merged Cells Yuan Zhao 16/05/2023 10:41:00

Merged Cells

Page 37: [15] Formatted Yuan Zhao 16/05/2023 10:41:00

Font: 9 pt

Page 37: [16] Merged Cells Yuan Zhao 16/05/2023 10:41:00

Merged Cells

Page 37: [17] Formatted Yuan Zhao 16/05/2023 10:41:00

Font: 9 pt

Page 37: [18] Merged Cells Yuan Zhao 16/05/2023 10:41:00

Merged Cells

Page 37: [19] Formatted Yuan Zhao 16/05/2023 10:41:00

Font: 9 pt

Page 37: [20] Merged Cells Yuan Zhao 16/05/2023 10:41:00

Merged Cells

Page 37: [21] Formatted Yuan Zhao 16/05/2023 10:41:00

Justified, Widow/Orphan control, Position: Horizontal: Centre, Relative to: Margin, Vertical: 0.61 cm, Relative to: Paragraph, Horizontal: 0.32 cm, Wrap Around

Page 37: [22] Formatted Yuan Zhao 16/05/2023 10:41:00

Font: 9 pt

Page 37: [23] Formatted Yuan Zhao 16/05/2023 10:41:00

Widow/Orphan control, Position: Horizontal: Centre, Relative to: Margin, Vertical: 0.61 cm, Relative to: Paragraph, Horizontal: 0.32 cm, Wrap Around

Page 37: [24] Formatted Yuan Zhao 16/05/2023 10:41:00

Font: 9 pt, Font colour: Black

Page 37: [25] Formatted Yuan Zhao 16/05/2023 10:41:00

Font: 9 pt

Page 37: [26] Formatted Yuan Zhao 16/05/2023 10:41:00

Font: 9 pt

Page 37: [27] Formatted Yuan Zhao 16/05/2023 10:41:00

Font: 9 pt

Page 37: [28] Formatted Yuan Zhao 16/05/2023 10:41:00

Justified, Widow/Orphan control, Position: Horizontal: Centre, Relative to: Margin, Vertical: 0.61 cm, Relative to: Paragraph, Horizontal: 0.32 cm, Wrap Around

Page 37: [29] Formatted Yuan Zhao 16/05/2023 10:41:00

Font: 9 pt

Page 37: [30] Formatted Yuan Zhao 16/05/2023 10:41:00

Widow/Orphan control, Position: Horizontal: Centre, Relative to: Margin, Vertical: 0.61 cm, Relative to: Paragraph, Horizontal: 0.32 cm, Wrap Around

Page 37: [31] Formatted Yuan Zhao 16/05/2023 10:41:00

Font: 9 pt, Font colour: Black

Page 37: [32] Formatted Yuan Zhao 16/05/2023 10:41:00

Font: 9 pt

Page 37: [33] Formatted Yuan Zhao 16/05/2023 10:41:00

Font: 9 pt

Page 37: [34] Formatted Yuan Zhao 16/05/2023 10:41:00

Font: 9 pt

Page 37: [35] Formatted Yuan Zhao 16/05/2023 10:41:00

Position: Horizontal: Centre, Relative to: Margin, Vertical: 0.61 cm, Relative to: Paragraph, Horizontal: 0.32 cm, Wrap Around

Page 37: [36] Formatted Yuan Zhao 16/05/2023 10:41:00

Font: 9 pt

Page 37: [37] Formatted Yuan Zhao 16/05/2023 10:41:00

Widow/Orphan control, Position: Horizontal: Centre, Relative to: Margin, Vertical: 0.61 cm, Relative to: Paragraph, Horizontal: 0.32 cm, Wrap Around

Page 37: [38] Formatted Table Yuan Zhao 16/05/2023 10:41:00

Formatted Table

Page 37: [39] Formatted Yuan Zhao 16/05/2023 10:41:00

Font: 9 pt, Font colour: Black

Page 37: [40] Merged Cells Yuan Zhao 16/05/2023 10:41:00

Merged Cells

Page 37: [41] Formatted Yuan Zhao 16/05/2023 10:41:00

Position: Horizontal: Centre, Relative to: Margin, Vertical: 0.61 cm, Relative to: Paragraph, Horizontal: 0.32 cm, Wrap Around

Page 37: [42] Formatted Yuan Zhao 16/05/2023 10:41:00

Font: 9 pt

Page 37: [43] Deleted Cells Yuan Zhao 16/05/2023 10:41:00

Deleted Cells

Page 37: [44] Formatted Yuan Zhao 16/05/2023 10:41:00

Font: 9 pt

Page 37: [45] Formatted Yuan Zhao 16/05/2023 10:41:00

Widow/Orphan control, Position: Horizontal: Centre, Relative to: Margin, Vertical: 0.61 cm, Relative to: Paragraph, Horizontal: 0.32 cm, Wrap Around

Page 37: [46] Formatted Yuan Zhao 16/05/2023 10:41:00

Font: 9 pt

Page 37: [47] Formatted Yuan Zhao 16/05/2023 10:41:00

Font: 9 pt

Page 37: [48] Inserted Cells Yuan Zhao 16/05/2023 10:41:00

Inserted Cells

Page 37: [49] Inserted Cells Yuan Zhao 16/05/2023 10:41:00

Inserted Cells

Page 37: [50] Inserted Cells Yuan Zhao 16/05/2023 10:41:00

Inserted Cells

Page 37: [51] Formatted Table Yuan Zhao 16/05/2023 10:41:00

Formatted Table

Page 37: [52] Inserted Cells Yuan Zhao 16/05/2023 10:41:00

Inserted Cells

Page 37: [53] Inserted Cells Yuan Zhao 16/05/2023 10:41:00

Inserted Cells

Page 37: [54] Inserted Cells Yuan Zhao 16/05/2023 10:41:00

Inserted Cells

Page 37: [55] Formatted Yuan Zhao 16/05/2023 10:41:00

Widow/Orphan control, Position: Horizontal: Centre, Relative to: Margin, Vertical: 0.61 cm, Relative to: Paragraph, Horizontal: 0.32 cm, Wrap Around

Page 37: [56] Formatted Yuan Zhao 16/05/2023 10:41:00

Font: 9 pt

Page 37: [57] Formatted Yuan Zhao 16/05/2023 10:41:00

Font: 9 pt

Page 37: [58] Formatted Yuan Zhao 16/05/2023 10:41:00

Don't adjust right indent when grid is defined, Widow/Orphan control, Don't snap to grid, Position: Horizontal: Centre, Relative to: Margin, Vertical: 0.61 cm, Relative to: Paragraph, Horizontal: 0.32 cm, Wrap Around

Page 37: [59] Formatted Yuan Zhao 16/05/2023 10:41:00

Font: 9 pt

Page 37: [60] Deleted Cells Yuan Zhao 16/05/2023 10:41:00

Deleted Cells

Page 37: [61] Deleted Cells Yuan Zhao 16/05/2023 10:41:00

Deleted Cells

Page 37: [62] Deleted Cells Yuan Zhao 16/05/2023 10:41:00

Deleted Cells

Page 40: [63] Formatted Yuan Zhao 16/05/2023 10:41:00

Line spacing: 1.5 lines

Page 40: [64] Formatted Yuan Zhao 16/05/2023 10:41:00

Line spacing: 1.5 lines

Page 40: [65] Formatted Yuan Zhao 16/05/2023 10:41:00

Font colour: Black

Page 40: [66] Formatted Yuan Zhao 16/05/2023 10:41:00

Font colour: Black

Page 40: [66] Formatted Yuan Zhao 16/05/2023 10:41:00

Font colour: Black

Page 40: [67] Formatted Yuan Zhao 16/05/2023 10:41:00

Font colour: Black

Page 40: [68] Formatted Yuan Zhao 16/05/2023 10:41:00

Font colour: Black

Page 40: [68] Formatted Yuan Zhao 16/05/2023 10:41:00

Font colour: Black

Page 40: [69] Formatted Yuan Zhao 16/05/2023 10:41:00

Font colour: Black

Page 40: [70] Formatted Yuan Zhao 16/05/2023 10:41:00

Font colour: Black

Page 40: [70] Formatted Yuan Zhao 16/05/2023 10:41:00

Font colour: Black

Page 40: [71] Formatted Yuan Zhao 16/05/2023 10:41:00

Font colour: Black

Page 40: [72] Formatted Yuan Zhao 16/05/2023 10:41:00

Font colour: Black

Page 40: [73] Formatted Yuan Zhao 16/05/2023 10:41:00

Line spacing: 1.5 lines

Page 40: [74] Formatted Yuan Zhao 16/05/2023 10:41:00

Font colour: Black

Page 40: [75] Formatted Yuan Zhao 16/05/2023 10:41:00

Font colour: Black

Page 40: [75] Formatted Yuan Zhao 16/05/2023 10:41:00

Font colour: Black

Page 40: [76] Formatted Yuan Zhao 16/05/2023 10:41:00

Font colour: Black

Page 40: [76] Formatted Yuan Zhao 16/05/2023 10:41:00

Font colour: Black

Page 40: [77] Formatted Yuan Zhao 16/05/2023 10:41:00

Font colour: Black

Page 40: [77] Formatted Yuan Zhao 16/05/2023 10:41:00

Font colour: Black

Page 40: [77] Formatted Yuan Zhao 16/05/2023 10:41:00

Font colour: Black

Page 40: [78] Formatted Yuan Zhao 16/05/2023 10:41:00

Font colour: Black

Page 40: [79] Formatted Yuan Zhao 16/05/2023 10:41:00

Font colour: Black

Page 40: [79] Formatted Yuan Zhao 16/05/2023 10:41:00

Font colour: Black

Page 40: [80] Formatted Yuan Zhao 16/05/2023 10:41:00

Font colour: Black

Page 40: [81] Formatted Yuan Zhao 16/05/2023 10:41:00

Font colour: Black

Page 40: [81] Formatted Yuan Zhao 16/05/2023 10:41:00

Font colour: Black

Page 40: [82] Formatted Yuan Zhao 16/05/2023 10:41:00

Line spacing: 1.5 lines

Page 40: [83] Formatted Yuan Zhao 16/05/2023 10:41:00

Font colour: Black

Page 40: [84] Formatted Yuan Zhao 16/05/2023 10:41:00

Font colour: Black

Page 40: [84] Formatted Yuan Zhao 16/05/2023 10:41:00

Font colour: Black

Page 40: [85] Formatted Yuan Zhao 16/05/2023 10:41:00

Font colour: Black

Page 40: [86] Formatted Yuan Zhao 16/05/2023 10:41:00

Font colour: Black

Page 40: [86] Formatted Yuan Zhao 16/05/2023 10:41:00

Font colour: Black

Page 40: [87] Formatted Yuan Zhao 16/05/2023 10:41:00

Font colour: Black

Page 40: [88] Formatted Yuan Zhao 16/05/2023 10:41:00

Font colour: Black

Page 40: [88] Formatted Yuan Zhao 16/05/2023 10:41:00

Font colour: Black

Page 40: [89] Formatted Yuan Zhao 16/05/2023 10:41:00

Font colour: Black

Page 40: [90] Formatted Yuan Zhao 16/05/2023 10:41:00

Line spacing: 1.5 lines

Page 40: [91] Formatted Yuan Zhao 16/05/2023 10:41:00

Font colour: Black

Page 40: [91] Formatted Yuan Zhao 16/05/2023 10:41:00

Font colour: Black

Page 40: [92] Formatted Yuan Zhao 16/05/2023 10:41:00

Font colour: Black

Page 40: [93] Formatted Yuan Zhao 16/05/2023 10:41:00

Font colour: Black

Page 40: [94] Formatted Yuan Zhao 16/05/2023 10:41:00

Font colour: Black

Page 40: [95] Formatted Yuan Zhao 16/05/2023 10:41:00

Font colour: Black

Page 40: [96] Formatted Yuan Zhao 16/05/2023 10:41:00

Font colour: Black

Page 40: [97] Formatted Yuan Zhao 16/05/2023 10:41:00

Line spacing: 1.5 lines

Page 40: [98] Formatted Yuan Zhao 16/05/2023 10:41:00

Font colour: Black

Page 40: [99] Formatted Yuan Zhao 16/05/2023 10:41:00

Font colour: Black

Page 40: [100] Formatted Yuan Zhao 16/05/2023 10:41:00

Font colour: Black

Page 40: [101] Formatted Yuan Zhao 16/05/2023 10:41:00

Font colour: Black

Page 40: [102] Formatted Yuan Zhao 16/05/2023 10:41:00

Font colour: Black

Page 40: [103] Formatted Yuan Zhao 16/05/2023 10:41:00

Font colour: Black

Page 40: [104] Formatted Yuan Zhao 16/05/2023 10:41:00

Font colour: Black

Page 40: [105] Formatted Yuan Zhao 16/05/2023 10:41:00

Font colour: Black

Page 40: [105] Formatted Yuan Zhao 16/05/2023 10:41:00

Font colour: Black

Page 40: [106] Formatted Yuan Zhao 16/05/2023 10:41:00

Line spacing: 1.5 lines

Page 40: [107] Formatted Yuan Zhao 16/05/2023 10:41:00

Font colour: Black

Page 40: [108] Formatted Yuan Zhao 16/05/2023 10:41:00

Font colour: Black

Page 40: [109] Formatted Yuan Zhao 16/05/2023 10:41:00

Font colour: Black

Page 40: [110] Formatted Yuan Zhao 16/05/2023 10:41:00

Font colour: Black

Page 40: [110] Formatted Yuan Zhao 16/05/2023 10:41:00

Font colour: Black

Page 40: [111] Formatted Yuan Zhao 16/05/2023 10:41:00

Font colour: Black

Page 40: [112] Formatted Yuan Zhao 16/05/2023 10:41:00

Font colour: Black

Page 40: [113] Formatted Yuan Zhao 16/05/2023 10:41:00

Font colour: Black

Page 40: [113] Formatted Yuan Zhao 16/05/2023 10:41:00

Font colour: Black

Page 40: [114] Formatted Yuan Zhao 16/05/2023 10:41:00

Line spacing: 1.5 lines

Page 40: [115] Formatted Yuan Zhao 16/05/2023 10:41:00

Font colour: Black

Page 40: [116] Formatted Yuan Zhao 16/05/2023 10:41:00

Font colour: Black

Page 40: [117] Formatted Yuan Zhao 16/05/2023 10:41:00

Font colour: Black

Page 40: [118] Formatted Yuan Zhao 16/05/2023 10:41:00

Font colour: Black

Page 40: [119] Formatted Yuan Zhao 16/05/2023 10:41:00

Font colour: Black

Page 40: [120] Formatted Yuan Zhao 16/05/2023 10:41:00

Font colour: Black

Page 40: [121] Formatted Yuan Zhao 16/05/2023 10:41:00

Font colour: Black

Page 40: [122] Formatted Yuan Zhao 16/05/2023 10:41:00

Font colour: Black

Page 40: [123] Formatted Yuan Zhao 16/05/2023 10:41:00

Line spacing: 1.5 lines